Contrib Mineral Petrol (2015) 170:15
DOI 10.1007/s00410-015-1169-9

ORIGINAL PAPER

Thermal metamorphism of mantle chromites and the stability of noble-metal nanoparticles

José M. González-Jiménez[1,2] · Martin Reich[1] · Antoni Camprubí[3] · Fernando Gervilla[4] · William L. Griffin[2] · Vanessa Colás[5] · Suzanne Y. O'Reilly[2] · Joaquín A. Proenza[6] · Norman J. Pearson[2] · Elena Centeno-García[3]

Received: 13 March 2015 / Accepted: 9 July 2015 / Published online: 30 July 2015

Abstract The Loma Baya complex in south-western Mexico is a volume of chromitite-bearing oceanic mantle that records a complex metamorphic history, defined by a first stage of hydrous metamorphism overprinted by a short-lived thermal event associated with an Eocene granite intrusion. During the hydrous metamorphism, the primary magmatic chromite–olivine assemblage was replaced by a secondary, porous intergrowth of Fe^{2+}-rich chromite and chlorite. The heat supplied by an Eocene-age granite intrusion reversed the hydration reaction, producing chromite rims with perfectly developed crystal faces. This third-generation chromite is in equilibrium with highly magnesian (neoformed) olivine and defines a chemical trend analogous to the original magmatic one. The preservation of both reactions in the Loma Baya chromitite provides compelling evidence that the hydration of chromite can be reversed by either prograde metamorphism or any heating event, confirming previous thermodynamic predictions. Understanding these complex features is of particular interest due to the fact that changes in temperature and variable degrees of fluid/rock interaction during metamorphism and intrusion have also significantly affected the chromite-hosted IPGE carrier phases. Here, we propose that the metamorphic fluids involved in the hydrous metamorphism have caused the desulphurization of laurite RuS_2, releasing minute particles of Ru–Os–Ir alloys <50 nm in diameter. The following short-lived thermal event that promoted dehydration in the chromitite had the opposite effect on nanoparticle stability, producing a significant coarsening of metal nanoparticles to dimensions larger than a micron. Based on such observations, we argue that IPGE nanoparticles can be exsolved and grown (or coarsen) from sulphide matrices during prograde metamorphism or heating and not exclusively upon cooling under magmatic conditions as it has been previously suggested. These results provide new insights on the relevant role of temperature and nanoparticle–host interaction phenomena in natural systems, shedding new light on the kinetic controls of nano- to micron-scale IPGE particle distributions during metamorphism.

Communicated by Othmar Müntener.

Electronic supplementary material The online version of this article (doi:10.1007/s00410-015-1169-9) contains supplementary material, which is available to authorized users.

✉ José M. González-Jiménez
jmgonzj@ing.uchile.cl

[1] Department of Geology and Andean Geothermal Center of Excellence (CEGA), Facultad de Ciencias Físicas y Matemáticas, Universidad de Chile, Plaza Ercilla # 803, Santiago de Chile, Chile

[2] ARC Centre of Excellence for Core to Crust Fluid Systems (CCFS) and GEMOC National Key Centre, Department of Earth and Planetary Sciences, Macquarie University, Sydney, NSW 2109, Australia

[3] Instituto de Geología, Universidad Nacional Autónoma de México, Ciudad Universitaria, 04510 México, D.F., Mexico

[4] Instituto Andaluz de Ciencias de la Tierra (Universidad de Granada-CSIC) and Departamento de Mineralogía y Petrología, Facultad de Ciencias, Universidad de Granada, Avda. Fuentenueva s/n, 18002 Granada, Spain

[5] Departamento de Ciencias de la Tierra, Universidad de Zaragoza, Pedro Cerbuna 12, 50009 Saragossa, Spain

[6] Departament de Cristal·lografia, Mineralogia i Dipòsits Minerals, Facultat de Geologia, Universitat de Barcelona, Martí i Franquès s/n, 08028 Barcelona, Spain

Keywords Chromite · Metamorphism · Nanoparticles · Noble metals

Introduction

A large body of data on platinum-group element (PGE) concentrations in basalts and komatiites allow predicting that Ir, as well as Ru and Os, are compatible with mantle minerals, playing sulphides and alloys the main role as host phases (e.g. Rëhkamper et al. 1999; Barnes and Fiorentini 2008; Park et al. 2013). This is consistent with experimental data showing that IPGE-bearing alloys and sulphides can form at mantle conditions (Brenan and Andrews 2001; Andrews and Brenan 2002; Brenan 2002; Bockrath et al. 2004a, b; Pruseth and Palme 2004; Fonseca et al. 2012) and with the fact that these minerals are commonly found in both exposed mantle fragments (i.e. peridotite massifs or abyssal peridotites; Mitchell and Keays 1981; Ohnenstetter 1992; Hutchinson et al. 1999; Lorand et al. 1999, 2010; Luguet et al. 2001, 2004, 2007) and mantle xenoliths (Alard et al. 2000, 2002, 2011; Wang et al. 2009). The Re–Os isotopic systematics of IPGE-rich sulphides and alloys occurring as inclusions in chromitites from oceanic mantle have been used to track the geochemical evolution of the upper convecting mantle (e.g. Malitch 2004; Ahmed et al. 2006; Shi et al. 2007; Marchesi et al. 2011; González-Jiménez et al. 2012a, 2013a, 2014). However, a large body of analytical and experimental evidence indicates that the chromitites may undergo significant alteration during metamorphism (Evans and Frost 1975; Burkhard 1993; Barnes 2000, 2001; Zaccarini et al. 2005; Mukherjee et al. 2010; Saumur and Hattori 2013; Barra et al. 2014). Commonly, hydrous alteration of chromite during metamorphism can lead to open-system conditions that may significantly disturb the original IPGE signatures in chromitite (Mondal et al. 2007; González-Jiménez et al. 2012b).

The most significant metamorphic modification of chromite is probably the formation of homogeneous, Fe^{3+}-rich rims (i.e. ferrian chromite) that often overgrow Fe^{2+}-rich porous chromite, defining a characteristic pattern of zoning that is interpreted to be the result of either prograde (Bliss and MacLean 1975; Evans and Frost 1975; Barnes 2000; González-Jiménez et al. 2009; Merlini et al. 2009; Saumur and Hattori 2013) or retrograde metamorphism (Proenza et al. 2004; Mellini et al. 2005; Gervilla et al. 2012; Barra et al. 2014; Merinero et al. 2014). However, thermodynamic modelling has recently shown that Fe^{2+}-rich porous chromite results from re-equilibration between igneous chromite and matrix olivine during the hydration of chromite-bearing ultramafic rocks (Gervilla et al. 2012; Barra et al. 2014). Therefore, the development of Fe^{2+}-rich porous chromite is a prerequisite for the formation of ferrian chromite via diffusion of Fe^{3+} into the pores of the previously formed porous chromite (Gervilla et al. 2012).

As noted above, the development of such porosity can have a significant impact on the stability of chromite-hosted IPGE carriers because it enhances fluid infiltration (González-Jiménez et al. 2012b, 2013b). In chromitites from the oceanic mantle, grains of laurite–erlichmanite (RuS_2–OsS_2) solid solutions are the main host phases for IPGE (González-Jiménez et al. 2014). The reaction of these magmatic laurites with metamorphic fluids usually produces secondary rims and/or nanometre to micrometre-sized inclusions of either (Os–Ir poor) Ru and/or (Ru poor) Os–Ir alloys via in situ desulphurization (Prichard and Tarkian 1988; McElduff and Stumpfl 1990; Nilsson 1990; Prichard et al. 1994, 2008; Zaccarini et al. 2005; Ghorfi et al. 2008; González-Jiménez et al. 2010). Previous compilations of electron microprobe analyser (EMPA) data of micron-sized grains of (Os–Ir poor) Ru alloys associated with S-deficient laurites in metamorphosed chromitites have shown that these particles have Ru/(Ru + Os + Ir) ratios identical to those of the coexisting (precursor) magmatic laurite, suggesting that they represent metallic "residues" after the selective leaching of Os, Ir and S from the sulphide (e.g. Stockman and Hlava 1984; Torres-Ruiz et al. 1996; Garuti and Zaccarini 1997). It has also been suggested that Os and Ir are released immediately after nucleation, based on the occurrence of nano- to micron-sized alloys at the reaction fronts, edges or margins of the larger precursor laurite grains (Zaccarini et al. 2005; Ghorfi et al. 2008; González-Jiménez et al. 2010). Note that the prefix "nano" is used in this work as a general term for fine particles or inclusions with sizes between 1 and 999 nm (the size below 1 μm) according to the conventional metric scale (i.e. measure of 10^{-9} units), rather than the sensu stricto definition of nanoparticle as those smaller than 100 nm (and larger than 1 nm) on the basis of the changes in the physical-chemical properties of the material (e.g. Hochella et al. 2008; SCENIHR 2010).

Recently, an increasing number of studies have reported the formation of nanocluster precursors and nanoparticles of PGEs under magmatic conditions (Bockrath et al. 2004a; Ballhaus et al. 2006; Finnigan et al. 2008; Kogiso et al. 2008; Helmy et al. 2013; Wirth et al. 2013; Junge et al. 2015). In their pioneering studies on the PGE–chromite–sulphide system, Bockrath et al. (2004a) and Ballhaus et al. (2006) documented the formation of nanoparticles of metallic Ru and Ir below the liquidus temperature (1200–1360 °C) in low-pressure (0.5 GPa) experiments. As a possible mechanism for the formation of such nanoalloys, Mungall (2002) and Finnigan et al. (2008) suggested that the IPGE alloys precipitated in response to small local perturbations in fO_2 of the parental melt. Reduction of the melt around the crystallizing chromite (by preferential

partitioning of Fe^{3+} and Cr^{3+} into the oxide phase) caused saturation in the most easily oxidized PGEs (Os, Ir, Ru) in the melt, which precipitate as metallic nanoparticles. Some authors have argued that these nanoparticles would be precursors of larger PGM sulphides (e.g. laurite) by reaction with S upon local increases of fS_2 in the melt (Tredoux et al. 1995; Bockrath et al. 2004a; González-Jiménez et al. 2009, 2012a, 2014). An alternative view suggests that the formation of IPGE-bearing sulphides and alloys (either of nano- or micron-sized) is related to the desulphurization of base-metal sulphides during partial melting at high temperature (Nakagawa and Franco, 1997; Peregoedova et al. 2004; Fonseca et al. 2012). In this model, a series of small events of melt extraction and melt-rock reaction may produce a progressive but stepped sequence of decreasing fS_2 in the mantle source region, promoting the breakdown of PGE-bearing base-metal sulphides into "residual" PGM sulphides (e.g. laurite), and to a major extent IPGE-bearing alloys (Shi et al. 2007; González-Jiménez et al. 2014).

However, unlike igneous systems where such studies are available, no information is currently available on the behaviour of IPGE nanoparticles at lower temperatures. Our current understanding of the stability of noble-metal nanoparticles under, e.g., metamorphic conditions typical of hydrous alteration of chromite and (hence) laurite relies almost exclusively on field studies, since only few experimental constraints are available (cf. Foustoukos et al. 2015). In particular, there is little knowledge on how size-confinement effects—i.e. changes in physical and chemical properties arising at the nanoscale—control the stability of noble-metal nanoparticles hosted by mineral phases at temperatures typical of the deep crust. Therefore, there is still great uncertainty on the details of the mechanisms that form IPGE metal particles and how they are preserved in the geological record.

Studies reporting the behaviour of noble metals in minerals analogue to laurite, e.g. pyrite, might provide a first approach to the problem of the formation/preservation of nanoparticles of IPGE alloys in natural laurites. In one of the very few studies reporting thermal stability of metal nanoparticles under crustal conditions, Reich et al. (2006) documented dramatic changes in the thermodynamic behaviour of gold nanoparticles incorporated in arsenian pyrite from refractory Au ores, thus confirming a relevant role for temperature-dependent nanoscale phenomena in geological systems. Native Au nanoparticles averaging ~4 nm in diameter were observed under the transmission electron microscope (TEM) during in situ heating to ~650 °C, showing that (1) gold nanoparticles remained unchanged from room temperature up to 370 °C, whereas (2) larger particles grew at the expense of smaller ones in an Ostwald-type ripening process above the aforementioned temperature. At 650 °C, only three nanoparticles (~30–35 nm) survived in the area of observation, formed by coarsening from the initial distribution of 115 particles of ~4 nm diameter. Upon cooling from 550 °C to room temperature, the particle growth processes were not reversed (Reich et al. 2006). Therefore, observations show that complete ripening of noble-metal nanoparticles (i.e. the final formation of a single large metal particle from a starting array of nanoparticles) may require temperatures of >550–600 °C to reach completion, setting an upper temperature and size limit for the occurrence of nanoparticulate Au in refractory sulphides.

In summary, naturally formed metal nanoparticles are subject to size and host effects that alter their thermal stability and control their occurrence in the geological record. Furthermore, the experiments by Reich et al. (2006) provide evidence that noble-metal nanoparticles can remain stable under higher temperatures within well-constrained conditions of temperature versus particle size. Therefore, and irrespective of the nature of the nanoparticle–host system, the size distribution of nanoparticles in refractory minerals may be considered as "snapshots" of transient regimes and may provide additional insights into the thermal history of the host rocks.

In this paper, we show evidence for the strong effect of temperature and mineral host alteration on the stability of noble-metal nanoparticle under metamorphic conditions. We make the first attempt to explain the formation and later preservation of nanoparticles of Ru–Os–Ir alloys in laurite from chromite-bearing rocks at Loma Baya, Mexico. This site is a key locality to study these effects because IPGE nanoparticle-bearing laurite grains have been modified by hydrous metamorphism followed by a superimposed short-lived thermal event. By combining mineralogical observations with geochemical data and thermodynamic modelling, we show that prograde metamorphism (or a heating event) superimposed on a porous Fe^{2+} chromite–chlorite assemblage gave rise to a new chromite assemblage and promoted significant changes in the IPGE-bearing hosts. This scenario provides a unique opportunity to compare the effects of thermal metamorphism on the composition of chromite and to explore how changes in temperature and variable degrees of fluid–rock interaction can impact the distribution of PGEs within chromite-hosted IPGE carrier phases. We also explore the potential effects of temperature, particle size and the texture of the host mineral on the stability of nanometre- to micrometre-sized particles of IPGE alloys in laurite. By constraining a general framework of nanoparticle-stability conditions, we aim to provide broad evidence of the relevant role of temperature and nanoparticle–host interaction phenomena and shed new light on the kinetic controls of small-scale IPGE distribution during metamorphism.

Geological background

The samples used in this study are massive chromitites from the Loma Baya ultramafic–mafic complex and were carefully selected since the chromite crystals have preserved the microstructural and chemical changes produced by metamorphism better than accessory chromite disseminated in the peridotites.

The Loma Baya ultramafic–mafic complex (~2 km long and 750 m wide) lies within the Zihuatanejo subterrane at the southernmost border of the Guerrero composite terrane (GCT), in the state of Guerrero, south-western Mexico (Fig. 1). It is one of the several mafic–ultramafic complexes of ophiolitic affinity that contain chromitite deposits along the boundaries of the GCT on the Pacific coast of Mexico (Ortiz-Hernández et al. 2006; Camprubí 2013). The Loma Baya ultramafic complex represents a portion of obducted subarc upper mantle, which probably formed in an intra-oceanic island arc developed during Late Jurassic to Early Cretaceous time along the palaeo-Pacific coast of Mexico (Mendoza 2000; Mendoza and Suastegui 2000; Ortiz-Hernández et al. 2006). Petrographic observations and mineral chemistry data on metasedimentary and metavolcanic rocks spatially associated with ultramafic rocks indicate that these rocks underwent early recrystallization during subduction at high pressure and low temperature (HP–LT) within the blueschist facies (200–330 °C and 0.5 to 0.7 GPa; Mendoza and Suastegui 2000). Metaultramafic rocks, chromitites and metamorphic rocks underwent a second stage of metamorphic re-equilibration (up to the amphibolite facies) during subsequent thermal metamorphism due to the intrusion of mid-Tertiary granites (Mendoza and Suastegui 2000).

The ultramafic portion of the Loma Baya complex consists of lenses of metadunite within porphyroclastic metaharzburgite; both were almost completely transformed to foliated serpentinites (i.e. schistose metaharzburgite) due to strong shearing and faulting. The mineral assemblages of these rocks consist mainly of antigorite with variable, although generally minor amounts of metamorphic olivine (~$Fo_{0.96}$; Table 1 of Supplementary material), tremolite, talc, chromium clinochlore and Cr-rich magnetite (up to 15 wt% Cr_2O_3). Olivine occurs as small (<250 μm) irregular grains scattered in the serpentine matrix and commonly hosts inclusions of serpentine and/or Cr-rich magnetite (Fig. 2a). Tremolite forms irregularly disseminated aggregates of subidiomorphic crystals (Fig. 2b). Talc tends to replace serpentine near olivine grain boundaries. Clinochlore occurs in the vicinity of relatively large, Cr-rich magnetite grains (100–300 μm) that are highly irregular in shape, often with corroded outlines and always fractured. Magnetite also occurs as minute (<50 μm), disseminated xenomorphic grains usually containing less Cr than larger ones. The metaultramafic rocks also contain dykes of diabase and microdiorite and are associated with mafic rocks, mainly gabbros. Along the contact between ultramafic and mafic rocks, a lens-like body that containing troctolites and hornblende pegmatites have yielded $^{40}Ar/^{39}Ar$ ages of ~38 Ma, consistent with resetting due to the intrusion of the Eocene granites (Fig. 1; Ferrari et al. 2014).

Blocks of massive chromitite were collected from dumps close to the old mining works from the Loma Baya chromite deposit (Salgado-Terán and Serrano-Villar 1983; Ortiz-Hernández et al. 2006). The chromitite body is hosted in a metadunite pod lying concordant with the foliation of the metaharzburgite and consists of massive chromite ore (>90 vol.% chromite). Further descriptions of the petrography and mineral compositions of the chromite are provided below.

Analytical methods

The samples were preliminarily inspected at the Geochemical Analysis Unit of CCFS/GEMOC (Macquarie University, Sydney, Australia) using a Zeiss EVO MAT 15 scanning electron microscope (SEM) equipped with energy-dispersive spectrometry and back-scattered electron (BSE) detectors. Major- and trace-element compositions of chromite and platinum-group minerals (PGMs) were obtained by wavelength-dispersive (WDS) analysis using a CAMECA SX100 electron microprobe (EMPA) at Macquarie University, Sydney, Australia, under the conditions described by González-Jiménez et al. (2013b).

Additional chromite and silicate grains were analysed by WDS using a CAMECA SX 50 at the Centres Científics i Tecnològics de la Universitat de Barcelona (CCiTUB) Barcelona, Spain. An acceleration voltage of 20 kV and a beam current of 15 nA were used, except for analyses of chromite, which required beam currents of 20 nA. Most elements were measured with a counting time of 10 s, except for Ni, V and Z (30 s). Representative data on silicate and chromite compositions are presented in Tables 1 and 2 of Supplementary material, respectively.

Analyses performed using EMPA with spot size of ~1 μm were sensitive to the presence of the nanometre- to micrometre-scale PGE alloy inclusions in pseudomorphs after laurite. As most of the analysed laurite grains contain such alloys and exhibit porosity, their analytical totals are usually very low (Table 3 of Supplementary material). This effect is inherent to porous grains and already been described in previous studies that report EMPA data of desulphurized laurites and/or porous Ru–Os–Ir alloys formed by low-temperature desulphurization of magmatic laurite (e.g. Stockman and Hlava 1984; Torres-Ruiz et al. 1996; Garuti and Zaccarini 1997; Proenza et al. 2007; González-Jiménez et al. 2010). Higher-total analyses of laurite were obtained in relatively homogeneous zones where nanometre-scale alloy inclusions were not detected under

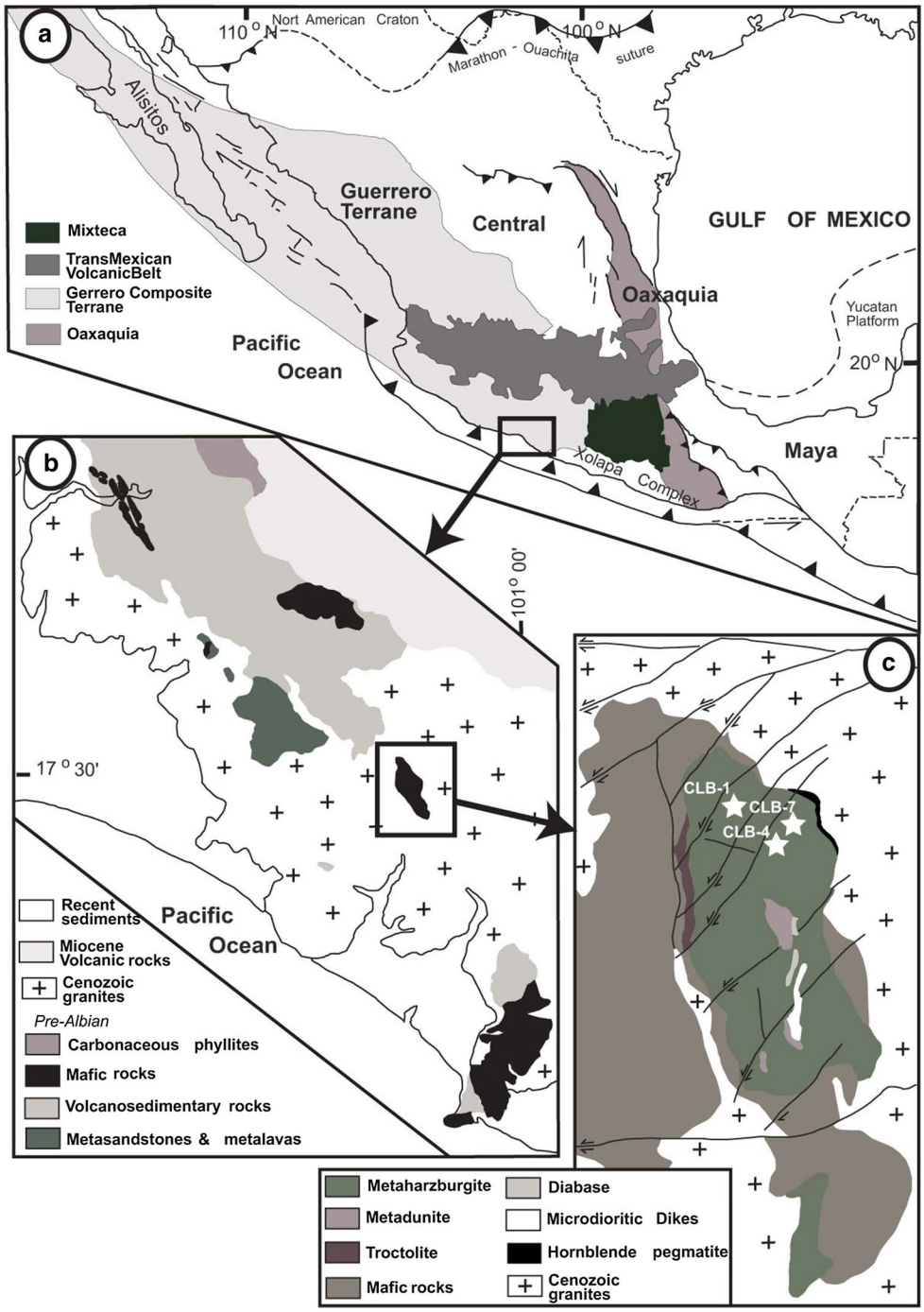

Fig. 1 **a** Geographic localization and main tectonic units of the Guerrero Terrane in Mexico. The *box* zoomed in **b** correspond to the Loma Baya ultramafic complex within the Zihuatanejo subterrane in south-western Mexico (**b**). **c** Simplified geological map of the Loma Baya ultramafic complex. Maps modified from Centeno-García et al. (2011). *White starts* indicate the location of the chromitite samples studied in this work

BSE, showing that all but one are S-deficient laurite grains (Table 3 of Supplementary material).

Thermodynamic modelling of phase relations during chromite alteration was performed using the Perple_X (Connolly 2009) with the thermodynamic database of Holland and Powell (1998, revised 2002) expanded to include Cr-bearing phases (cr_hp02ver.dat). The components considered in the closed system were Cr_2O_3–MgO–FeO–Al_2O_3–SiO_2–H_2O (CrMASH), and the considered solid solutions are the Cr-spinel (Klemme et al. 2009), olivine and chlorite (Holland and Powell 1998). The Cr-spinel solid solution is restricted to binary mixing between Cr and Al in the octahedral site and between Mg and Fe^{2+} in the tetrahedral site. Mixing properties used in Perple_X for the octahedral site are based on the subregular solution proposed by Oka et al. (1984), and for tetrahedral sites, the ideal solution model proposed by Engi (1983) is used. Chromium-bearing chlorite was not considered since

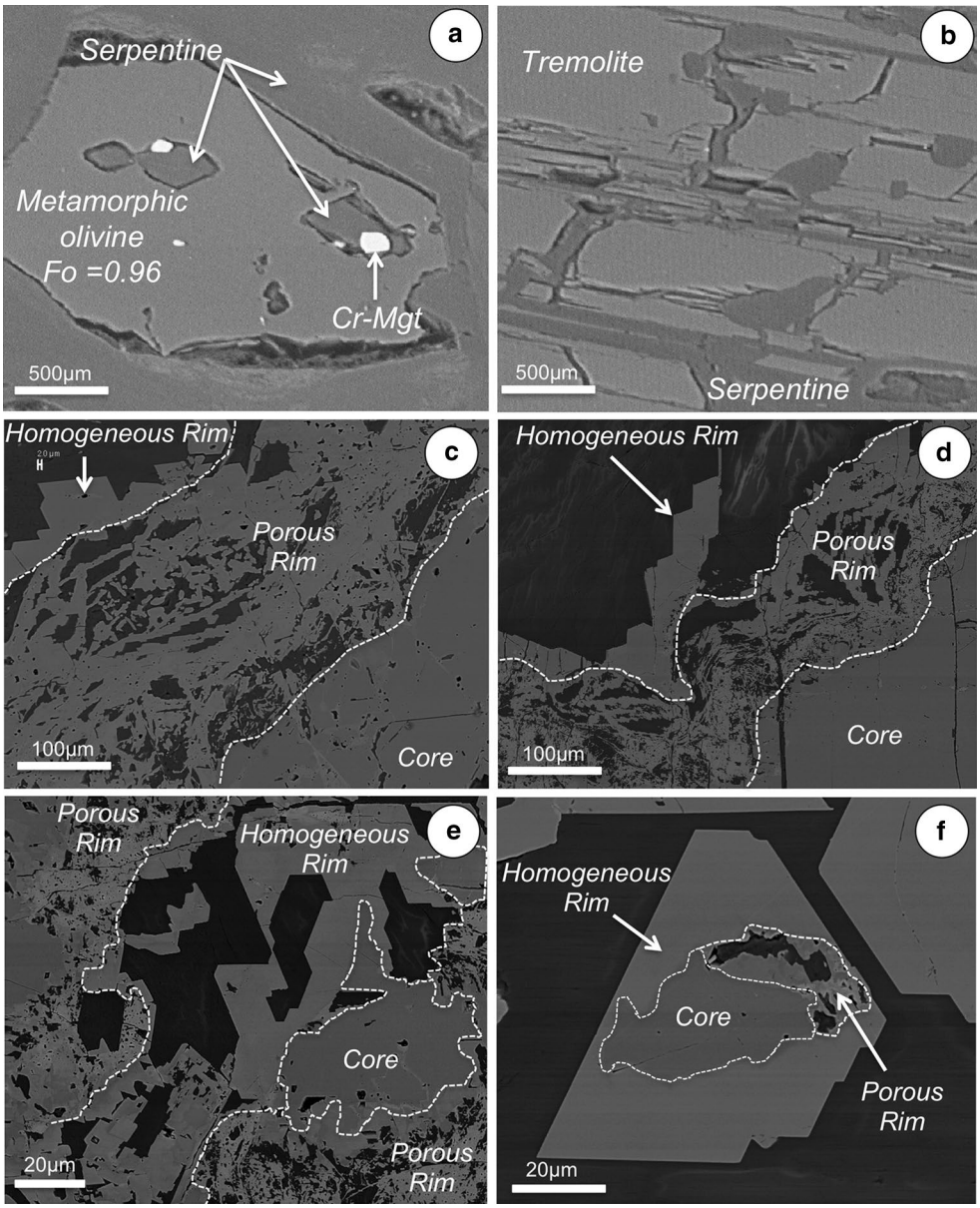

Fig. 2 Backscattered-electron images of silicate relationships in host serpentinite (**a, b**) and chromite structure in massive chromitite at Loma Baya. **a** Assemblage of serpentine + Cr-rich magnetite replaced by a larger porphyroblast of olivine embedded in serpentine. **b** Intergrowth of tremolite and serpentine. **c–f** Examples of magmatic chromite (*darker cores*) surrounded by the two metamorphic rims (porous and homogeneous) identified in this study

experimental data on mixing parameters for Al, Cr, Mg and Fe^{2+} in this phase are currently unavailable in the literature.

Results

Chromite zoning

Chromite modal abundance varies from 90 to 98 % in the studied chromitites. The grains are hypidiomorphic and range between 0.5 and 3 cm in diameter. The matrix between the chromite grains consists of clinochlore and rare, minute crystals of rutile. Most chromite grains exhibit a thick network of fractures and show optical and chemical zoning under petrographic and SEM–BSE observation, respectively (Fig. 2c–f). Under SEM–BSE, zoning in single chromite grains is defined by the presence of darker cores (the innermost part of the grain), with rounded and irregular morphology. Such cores are surrounded by rims of variable thickness of porous and/or homogeneous chromite in some of the largest crystals (Fig. 2c–f). Porous chromite rims show higher reflectivity than cores and contain

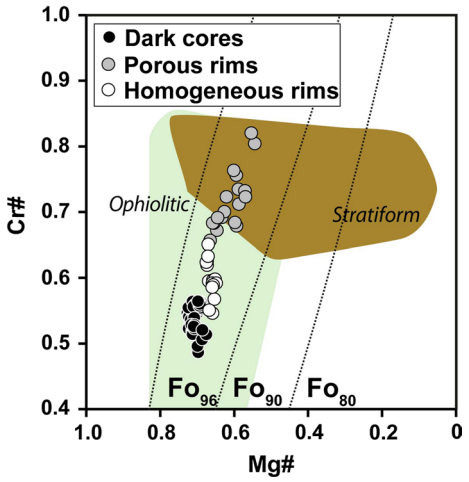

Fig. 3 Chemical variations of chromite at Loma Baya in terms of Cr# [Cr/(Cr + Al) atomic ratio] versus Mg# [Mg/(Mg + Fe^{2+}) atomic ratio]. Fields of chromite in chromitites of the "ophiolitic type" and "stratiform mafic intrusions type" (Leblanc and Nicolas 1992) are included for comparison

abundant xenomorphic inclusions of serpentine and chlorite (Fig. 2; Table 1 of Supplementary material). Homogeneous chromite rims show reflectivity intermediate between those of the dark cores and the porous rims. Overall, homogeneous rims form the external zone of the chromite grains and consist of euhedral chromite (Fig. 2f) often with polygonal habit; they contain no chlorite but very small euhedral inclusions of olivine. After detailed petrographic inspection of several samples, the presence of the three described microtextural varieties (dark core ⇒ porous rim ⇒ homogeneous rim) was only observed in larger chromite grains; the transition between dark cores and the two rims (porous or homogeneous) can either be sharp or gradational.

Dark chromite cores show almost constant low Cr# [Cr# = (Cr/(Cr + Al) atomic ratio = 0.49–0.56] and high Mg# [Mg# = (Mg/(Mg + Fe^{2+}) atomic ratio = 0.68–0.73] (Table 2 of Supplementary material). Such values are similar to those shown by the primary high-Al chromite of many ophiolitic chromitites and represent the most primitive (i.e. magmatic) composition (Fig. 3). These ratios become more variable in porous chromite rims where Cr# ranges between 0.66 and 0.82 and Mg# between 0.55 and 0.67. The homogeneous rims show composition intermediate between those of dark cores and porous rims (Cr# = 0.55–0.65 and Mg# = 0.65–0.68; Fig. 3).

Most minor oxides (TiO_2, NiO, MnO and ZnO) show small variations from unaltered chromite to porous and homogeneous rims. TiO_2 contents are slightly higher in unaltered (0.03–0.21 wt%) than in porous (0.04–0.15 wt%) or homogeneous chromite (0.04–0.13 wt%). Similarly, NiO contents vary from 0.08–0.23 wt% in unaltered chromite to 0.03–0.13 wt% in porous rims and to <0.12 wt% in homogeneous rims. In contrast, MnO contents increase significantly from unaltered chromite (0.3–0.6 wt%) to porous rims (0.6–1.0 wt%) and decrease from porous to homogeneous rims (0.5–0.6 wt%). ZnO contents in the three microstructural types of chromite are similar, ranging between 0.01 and 0.55 wt%.

Micron-sized inclusions and nanoparticles of PGE alloy in pseudomorphs of laurite

Twenty-six grains of laurite (RuS_2) were identified in the studied chromite grains, and all except one were found outside of the darker primitive cores (Fig. 4a–i). This single laurite grain is fully enclosed in a dark core and shows a homogeneous composition with almost stoichiometric atomic proportions (Table 3 of Supplementary material). The other laurite grains were found in chromite rims (Fe^{2+}-rich porous chromite and homogeneous chromite) and in the chlorite matrix; these are actually pseudomorphs of laurite that now consist of a matrix of S-poor laurite (Table 3 of Supplementary material) dusted with abundant nanometre- to micrometre-sized inclusions of metallic Ru–(Os–Ir) alloys (Fig. 4b–h). Such laurite pseudomorphs usually preserve the euhedral shape of the magmatic laurite (Fig. 4b) but often show irregular outlines as they adapt to the morphology of micropores that formed during the alteration of their chromite host (e.g. Fig. 4b, c) or matrix chlorite (Fig. 4f).

Under high magnification and SEM–BSE observation, laurite shows abundant nanometre- to micrometre-sized particles of Ru–(Os–Ir) alloys, whose composition were confirmed using EDS analysis (Fig. 4). Such grains and particles appear bright against the lower average atomic mass of the laurite matrix. An estimation of their approximate composition was obtained from raw EMPA analysis of clusters of these nanometre- to micrometre-sized particles, subtracting the composition of the host laurite. All these PGM particles consist of Ru with variable proportions of Ir or Os (Table 3 of Supplementary material), and their size and distribution vary depending on the internal organization of the laurite host.

In laurite pseudomorphs that contain micrometre-sized pores and/or a dense fracture network, a myriad of nanometre-sized inclusions of PGE alloys usually cluster in micrometre-sized pores (e.g. Fig. 4b). The abundant Ru–(Os–Ir) nanoparticles in the laurite pseudomorphs have rounded shapes, average diameters of ~110 nm and modal abundances of ~60 nm (Fig. 5a). They also tend to occur at the cores of laurite grains and agglomerate at the intersection between fractures, giving a vermicular aspect at lower, micrometre-scale magnification (Fig. 4c, g, h). Some of the laurite pseudomorphs exhibit more intricate microstructures in which homogeneous nanoparticle-free S-deficient

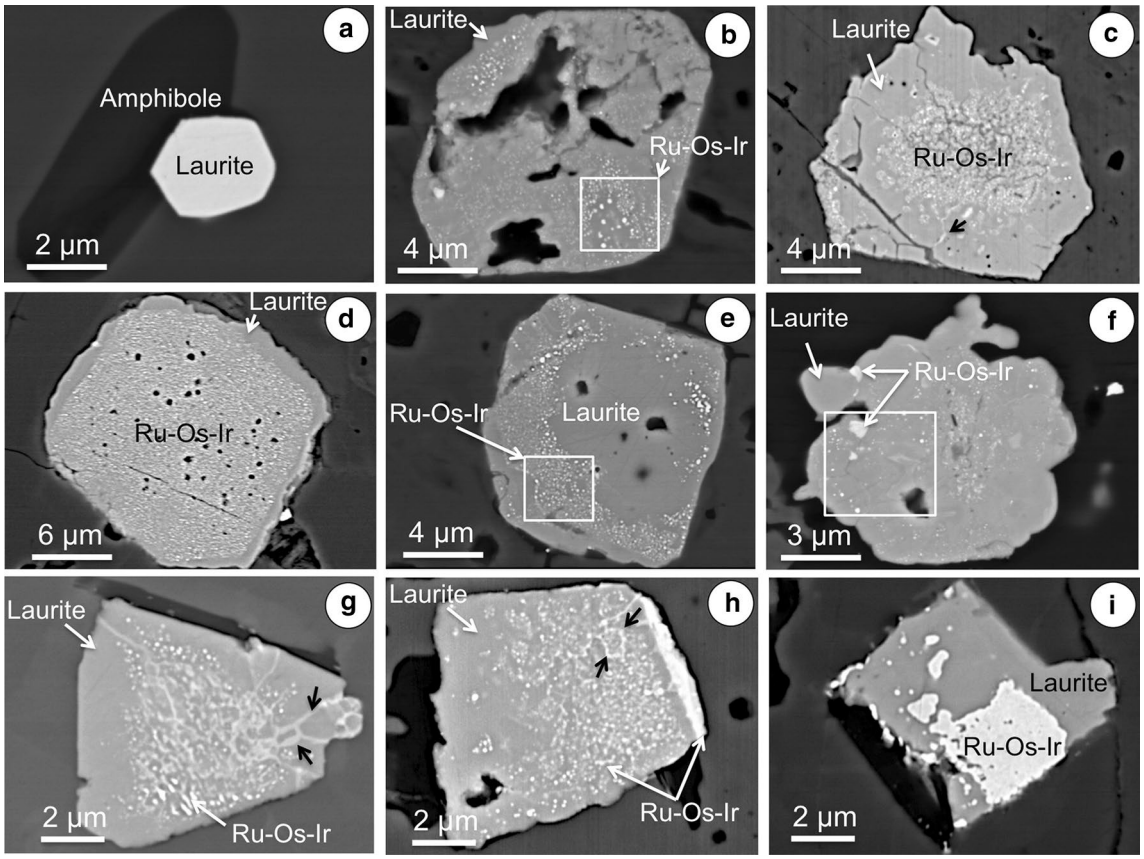

Fig. 4 Backscattered electron images of laurite (**a**) and pseudomorphs of laurite (**b–i**) hosting nanometre- and micrometre-sized particles of Ru–(Os–Ir) alloys in the Loma Baya chromitites. Image **a** a pristine (magmatic) laurite is protected from alteration by enclosure in an unaltered chromite crystal. Images **b–i** show altered and partly desulphurized laurites (i.e. S-deficient laurite) in metamorphic rims of chromite. *Black arrows* indicate preferential zones of nanometre-sized particles coalescing to form nanometre-sized channels. *White squares* indicate the areas we used as representatives for the analysis of size distribution of the Ru–(Os–Ir) particles

laurite cores or rims (concentric or irregular, patchy zones) alternate with zones that contain abundant Ru–(Os–Ir) nanoparticles (Fig. 4d, e). Nanoparticles in such zones have approximate average diameters and modal abundances of ~110 and ~90 nm, respectively (Figs. 4e, 5b).

In contrast, in laurite pseudomorphs where micrometre-sized pores are much less abundant or absent (e.g. Fig. 4f), Ru–(Os–Ir) nanoparticles clump to form particle aggregates with variable average sizes (Fig. 4h–i). Some nanoparticles grow to over 500 nm in diameter and develop increasingly irregular shapes (Figs. 4f, 5c). Size distributions of the Ru–(Os–Ir) nanoparticles in laurite pseudomorphs are bimodal, where larger particles >100 nm in diameter coexist with more abundant particles of sizes smaller than 100 nm across (Figs. 4f, 5c). In some cases, nanoparticles may agglomerate to form interconnected networks of veins within the laurite matrix (Fig. 4g–h). As the veins coalesce towards the edge of laurite grains, they can produce larger micrometre-sized inclusions of Ru–(Os–Ir) alloys (Fig. 4h).

Discussion

Metamorphic zoning in chromite

As previously noted, zoned chromite grains that consist of mostly unaltered cores enveloped by chemically distinct porous and/or homogeneous rims of variable thickness are common features of primary chromite modification during metamorphism (Golding and Bayliss 1968; Bliss and MacLean 1975; Evans and Frost 1975; Wylie et al. 1987; Thalhammer et al. 1990; Suita and Streider 1996; Barnes 2000, 2001; Proenza et al. 2004; González-Jiménez et al. 2009; Mukherjee et al. 2010; Gervilla et al. 2012; Saumur and Hattori 2013; Barra et al. 2014). In the studied samples, the overgrowth of homogeneous chromite with inclusions of metamorphic olivine on the rims of porous chlorite-bearing Fe-$^{2+}$-rich chromite provides persuasive evidence that the zoning in the chromite is not igneous in origin (Fig. 2c–f). This is consistent with the occurrence of

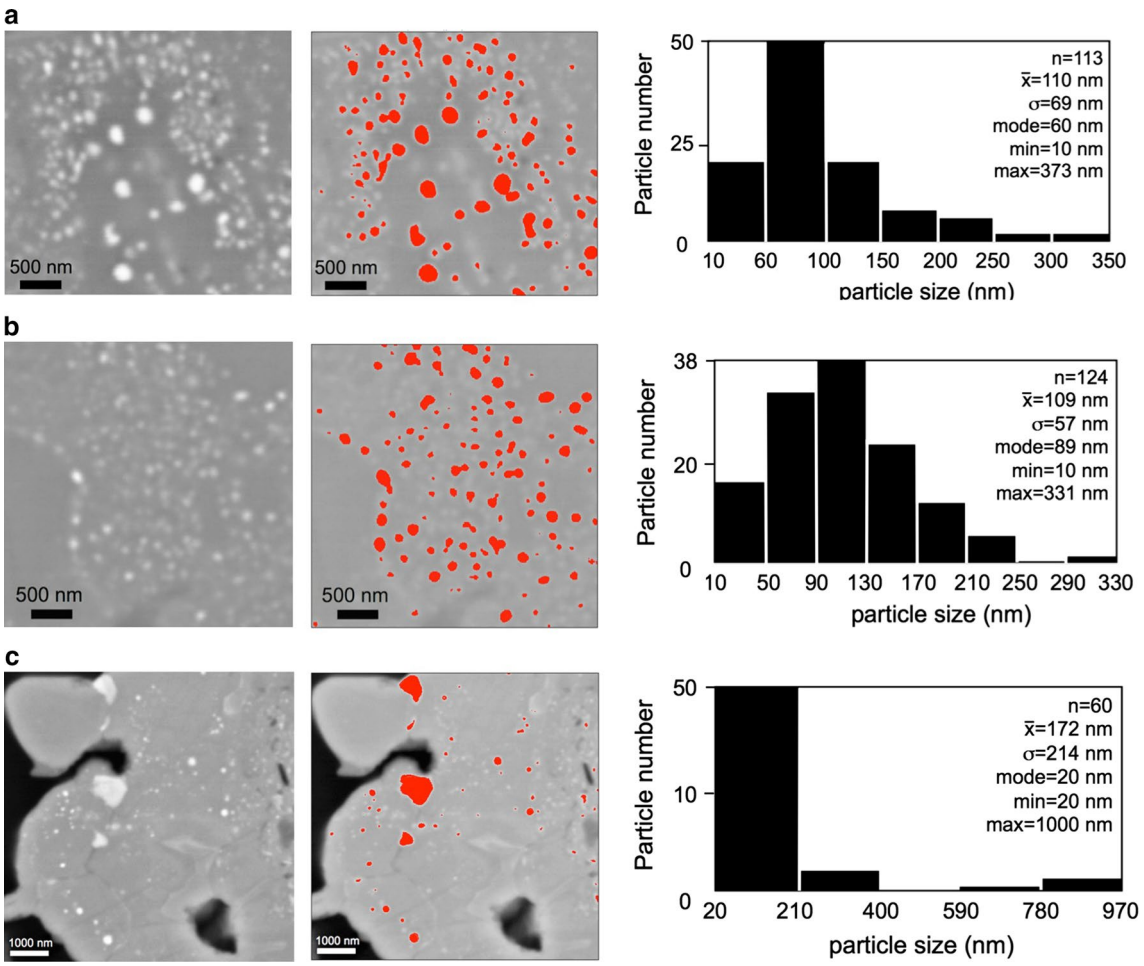

Fig. 5 Particle-size distributions of nanometre-scale Ru–(Os–Ir) alloys hosted in laurite grains from Loma Baya. **a–c** correspond to enlarged areas in Fig. 4b, e, f, respectively. The approximate particle-size distribution was obtained from SEM–BSE image analysis using the ImageJ software (Schneider et al. 2012). For each panel, the original BSE image is shown on the *left side*, a threshold image showing nanoparticles in *red* (false) colour is included in the centre, and a histogram is shown on the *right side*. In the latter, statistical particle-size parameters are shown (average, standard deviation, mode and maximum and minimum sizes). Particle size was calculated as Feret's diameter (or calliper length), which is the longest distance between any two parallel tangents to the projected outline of the particle

an assemblage of antigorite, tremolite, talc, chlorite and Cr-rich magnetite within the host rock (Fig. 2a, b), which is stable at low pressures and temperatures typical of amphibolite facies metamorphism.

In the zoned chromite from Loma Baya, the composition of the dark cores can be considered as representative of the original magmatic composition. This assumption is supported by low Fe_2O_3 contents (<5 wt%; i.e. $[Fe^{3+}\# = Fe^{3+}/(Fe^{3+}+Al+Cr)] < 0.06$) and high MgO (>15 wt%). This is the composition expected for chromian spinel in equilibrium with Fo_{93-95} olivine at 1200 °C (Fig. 3; Dick and Bullen 1984) and is typical of mantle-hosted ophiolitic chromitites (González-Jiménez et al. 2014 and references therein). In contrast, a trend of Al_2O_3 loss followed by MgO loss that is characteristic of Fe^{2+}-rich porous chromite (Fig. 3) can be associated with a the preferential partitioning of these elements towards secondary chlorite (clinochlore) that crystallized in the pores left in chromite.

Merlini et al. (2009) explained the formation of Fe^{2+}-rich porous chromite in equilibrium with chlorite as the result of the reaction of chromite with antigorite during prograde metamorphism that post-dated serpentinization:

$$\begin{aligned} &2\underset{\text{chromite}}{\left(Mg_{0.60}Fe_{0.40}\right)\left(Cr_{1.30}Al_{0.70}\right)O_4} \\ &\quad + 3/2\underset{\text{antigorite}}{\left(Mg_{2.57}Al_{0.32}Fe_{0.11}\right)Si_2O_5(OH)_4} + H_2O + 1/12O_2 \\ &\Rightarrow 7/6\underset{Fe^{2+}\text{-rich chromite}}{\left(Mg_{0.40}Fe_{0.60}\right)\left(Cr_{1.85}Fe_{0.08}Al_{0.07}\right)O_4} \\ &\quad + 1/2\underset{\text{Cr-clinochlore}}{\left(Mg_{9.18}Fe_{0.34}Al_{1.60}Cr_{0.88}\right)\left(Al_2Si_6\right)O_{20}(OH)_{16}} \end{aligned} \quad (1)$$

However, this equation that is based on the reaction of a primary chromite is richer in Cr_2O_3 than that found at Loma Baya and is not in agreement with phase relations in the fluid saturated Cr_2O_3–MgO–FeO–Al_2O_3–SiO_2–H_2O (CrMFASH) system for Al-rich rocks such as chromitites (see Fig. 6 in Gervilla et al. 2012). This precludes the formation of high-Cr chromite and chlorite by the breakdown of antigorite and high-Al chromite as suggested by Merlini et al. (2009).

Figure 6a shows an isochemical diagram (pseudosection) in the system CrMFASH for an initial dry assemblage of 90 % chromite and 10 % olivine (molar mix). We assume water-saturated conditions, an average dark chromite core of $(Mg_{0.7}Fe_{0.3})Cr_{1.08}Al_{0.92}FeO_4$ and Fo_{94}, for the olivine in equilibrium with chromite at 1200 °C (Fig. 3; Dick and Bullen 1984). Our modelling predicts that the maximum slope is located between ~700 °C (at 4 GPa) and 300 °C (at 0.2 GPa), thus predicting that under water-saturated conditions, magmatic chromite in massive chromitites is not stable with olivine below 700 °C. At these conditions, the stable assemblage is made up of chromite with higher Cr# and lower Mg# in equilibrium with clinochlore, brucite and diaspore, depending on pressure and temperature (Fig. 6a–c). Our model also predicts that porous chromite with Cr # = 0.82 and Mg# = 0.55 in massive samples as in Loma Baya should form at ~330 °C and 0.7 GPa (Fig. 6b, c), which fits well with the P–T conditions that estimated for the metamorphic peak in the metamorphic rocks that are spatially associated with the ultramafic complex at Loma Baya.

This suggests that Fe^{2+}-rich porous chromite in the massive chromitites at Loma Baya is the result of re-equilibration between high-Al chromite and olivine when aqueous fluids infiltrated the mantle peridotite during (mainly) metamorphism within the blueschist facies. The replacement of olivine and chromite alteration could be expressed by the simplified reaction:

$$\underset{\text{Chromite}}{4(Mg_{0.7}Fe_{0.3})CrAlO_4} + \underset{\text{Forsterite}}{4(Mg_{1.88}Fe_{0.12})SiO_4} + 2SiO_{2aq.} + 8H_2O \rightarrow \underset{\text{Clinochlore}}{2(Mg_{4.61}Fe_{0.39})AlSi_3AlO_{10}(OH)_8} + \underset{Fe^{2+}\text{-rich chromite}}{2(Mg_{0.55}Fe_{0.45})Cr_2O_4} \quad (2)$$

Reaction 2 is a modified version of those proposed by Gervilla et al. (2012) and Barra et al. (2014), which use a reacting primary chromite with high-Al contents, similar to the one studied in this paper. This reaction proceeds under water-saturated conditions, and the high silica activity in hydrous fluids is justified by the presence of tremolite in the mineral assemblage. Also, a relatively high proportion of silica in the system can explain the lack of brucite in the host-rock metamorphic assemblage (Frost and Beard 2007; Jöns et al. 2010; Frost et al. 2013; Foustoukos et al. 2015). Furthermore, contrary to the prediction of the thermodynamic model, we did not identify diaspore in the mineral assemblage, which can be explained as a consequence of the excess of alumina in the system, which was taken up by chlorite. The porous texture in the secondary Fe^{2+}-rich chromite is interpreted as the consequence of mass loss and volume reduction of chromite grains due to the preferential partitioning of Al_2O_3 and MgO into clinochlore (Merlini et al. 2009; Gervilla et al. 2012).

It is worth to note that in Reaction 2, the amount of primary chromite that is altered is directly related to the amount of olivine in the chromitite or host rock; i.e. 4 mol of primary must react with 4 mol of olivine to produce 2 mol of secondary chromite. This is consistent with the observation that chromite grains in massive chromitites (i.e. high chromite/silicate ratios) are usually less altered than those of semimassive or disseminated chromitites (i.e. lower chromite/silicate ratios), even if all them have undergone a common metamorphic pathway (e.g. González-Jiménez et al. 2009; Mukherjee et al. 2010). Our thermodynamic model's prediction does not exclude the possibility that external MgO- and SiO_2-rich fluid, most likely derived from peridotitic country rocks, could also promote the formation of secondary porous chromite and chlorite after primary chromite. However, in the case of Loma Baya, the sole consumption of the olivine matrix of the chromitite (i.e. 10 % vol.) may explain the formation of observed thin rims of secondary porous chromite. An additional supply of Mg and Si by external fluids once olivine matrix has been exhausted from the chromitite rock may explain the almost complete replacement to secondary porous chromite, as described in other metamorphosed chromitites.

Significantly, the overgrowth of homogeneous rims on porous rims or directly on unaltered chromite cores suggests a change in metamorphic conditions (Fig. 6a). The homogeneous chromite rims have lower Cr# (0.55–0.65) and higher Mg# (0.65–0.68) than Fe^{2+}-rich porous chromite, thus turning back towards the composition of primary chromite (Fig. 3). According to our calculated phase relations, the increase in Al and Mg could be related to the breakdown of chlorite, if a change in the metamorphic conditions occurred in the direction opposite to reaction 2: Fe^{2+}-rich porous chromite reacts with pore and/or matrix chlorite, thus forming homogeneous chromite with a composition close to that of the unaltered cores and olivine. Chlorite is very rare or absent in the homogeneous rims, whereas such rims contain minute inclusions of highly magnesian olivine (Fo_{96}; Table 1 of Supplementary material). In the ultramafic host rock, this olivine grows at expense of antigorite and, to a lesser extent, of Cr-rich magnetite (Fig. 2a). Our thermodynamic modelling is also consistent with petrographic observations, because it predicts that highly magnesian olivine ($Fo_{95–96}$) is in equilibrium

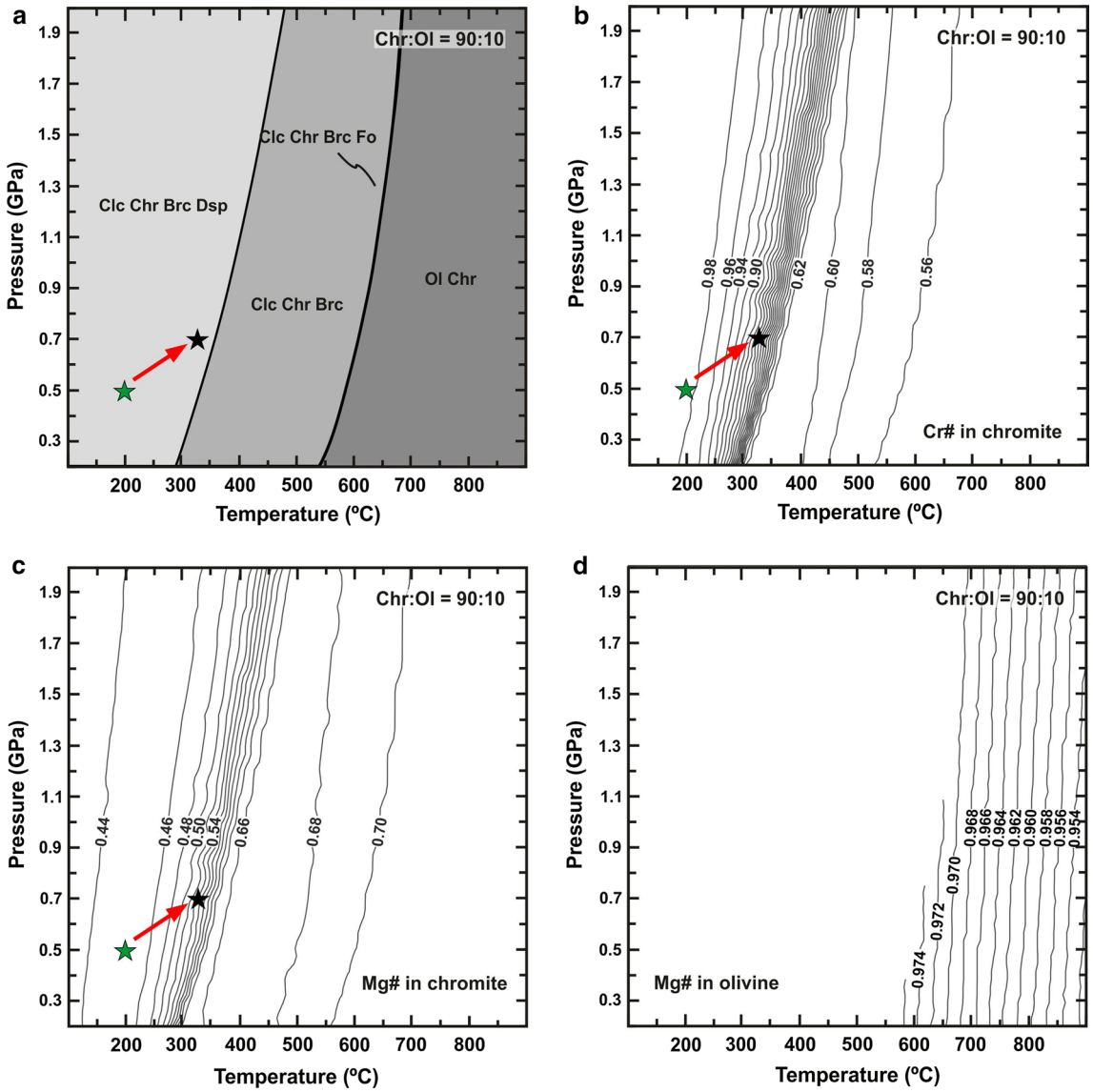

Fig. 6 **a** Isochemical phase diagram (pseudosection) calculated for a model chromitite composition in the CrMFASH system for 90:10 chromite–olivine molar proportions. Isopleths calculated for the same system and proportions of chromite–olivine are shown for Cr# and Mg# (mole proportion) in chromitites in **b** and **c**, respectively, and for Mg# (mole proportion) in olivine in **d**. Stars and red arrow indicate the P–T path proposed by Mendoza (2000) in metamorphic rocks associated with the Loma Baya ultramafic complex

with chromite with the same composition as the metamorphic homogeneous chromite rims identified in this study (Fig. 6d).

These observations are consistent with dehydration of the antigorite serpentinite host rock. The common range of PT conditions where dehydration reactions of antigorite are reported extends from less than 0.4 GPa at <570 °C (contact metamorphism; Trommsdorff and Evans 1972; Springer 1974; Frost 1975; Arai 1975; Matthes and Knauer 1981; Paktunç 1984; Worden et al. 1991; Trommsdorff and Connolly 1996; Ulmer and Trommsdorff 1995, 1999; Nozaka 2003; Nagaya et al. 2014) to over 2 GPa at >680 °C (high-grade regional metamorphism; Trommsdorff and Evans 1974; Khedr and Arai 2010, 2012; Padrón-Navarta et al. 2010). However, it is unlikely that the observed dehydration reactions of the ultramafic rocks in this study are related to regional metamorphism. The ultramafic complex of Loma Baya is in close contact with younger granitic batholith, and thermal metamorphism of the ultramafic rocks by the granitic intrusive is illustrated by resetting of the $^{40}Ar/^{39}Ar$ age of pegmatites associated with these ultramafic rocks (Delgado-Argote et al. 1992).

Granitic magmas are usually emplaced at low pressures (0.2–0.35 GPa) in the mid-shallow crust at ~700–750 °C.

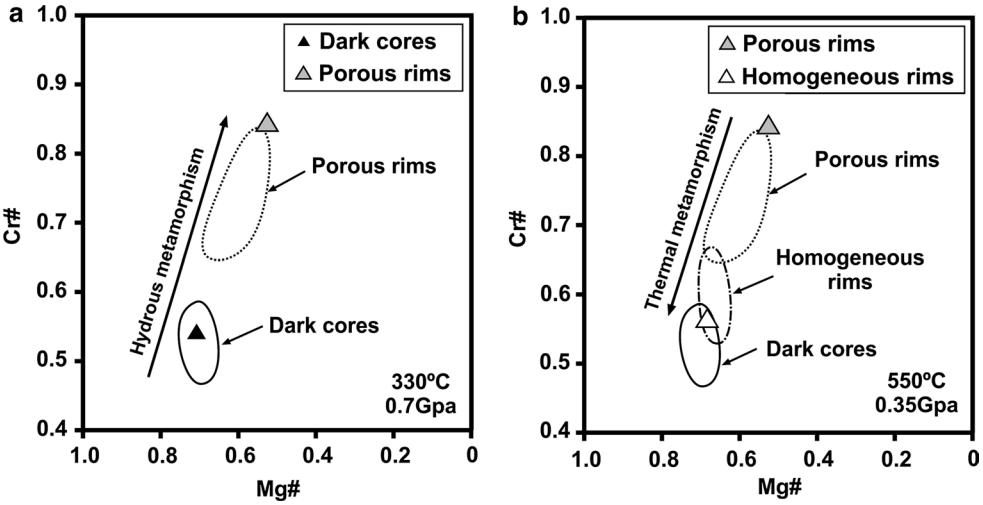

Fig. 7 Plots Cr# versus Mg# showing the composition of porous chromite and homogenous predicted by our thermodynamic model (*grey* and *white* triangles, respectively) at the peak of hydrous (330 °C and 0.7 GPa) and thermal metamorphism (550 °C and 0.35 GPa) estimated for the Loma Baya ultramafic complex. The fields represent the composition of natural chromites in the Loma Baya chromitites

When these magmas intrude serpentinites, they usually produce contact aureoles with well-defined metamorphic zoning and mineral assemblages in the ultramafic body (Trommsdorff and Evans 1972; Springer 1974; Arai 1975; Trommsdorff and Connolly 1996). From experimental studies and thermodynamic calculations (e.g. Evans et al. 1976; Worden et al. 1991), we know that at 0.2–0.35 GPa, antigorite reacts to produce olivine + talc + H_2O at about 515–570 °C in the pure MSH system. Similar temperatures are obtained using a mixed silica-richer CMSH system in which an antigorite + olivine + tremolite + chlorite assemblage would react to produce talc and H_2O, at the expenses of antigorite, at ~530 °C and 0.2 GPa (Trommsdorff and Connolly 1996). These thermal conditions for the low-pressure dehydration reaction of antigorite apply well to the Loma Baya serpentinites, which were very likely derived from a dunitic and harzburgitic protolith. Interestingly, our estimations from the CrMFASH predicts that at the given pressures of <0.35 GPa, highly magnesian olivine ($Fo_{95–96}$) must be in equilibrium with chromite having Cr# of 0.56–0.57 and Mg# of 0.69 at ~550 °C (Fig. 6). If the uncertainty in the mixing model of spinels is considered, this predicted composition fits well with the composition of the homogenous chromite at Loma Baya (Cr# 0.55–0.65 and Mg# = 0.65–0.68; Fig. 7).

Thermal profiles computed by Trommsdorff and Connolly (1996) in the Bergell aureole (north Italy) predicts the existence of a zone of antophyllite + olivine, which would be produced at expenses of talc at ~633 °C, within ~1000 m away from the contact with the granitic intrusion. However, we have not observed such assemblage in our rocks. As a result, a temperature of approximately 550–600 °C, obtained from chromite–olivine pairs in the chromitites and silicate assemblages in their host rocks, can bracket the prograde metamorphic peak in the Loma Baya ultramafic complex. Also, the preservation of Fe^{2+}-rich porous chromite rims in some of the studied chromite samples suggests that the heating event was very limited in time and/or restricted to the proximity of the granite intrusion, thus precluding the complete replacement of the pre-existing chromite textures. However, more detailed studies are required to validate this statement.

On the other hand, the absence of secondary base-metal minerals (such as arsenides, sulpharsenides, stannides or antimonides), which have been observed in other thermally metamorphosed ultramafic bodies, rules out the infiltration of external fluids derived from the granitic intrusion (e.g. Arai et al. 1999; Garuti et al. 2007). Instead, the local formation of homogeneous chromite rims is associated with the migration of hot fluids towards the central part of the ultramafic complex; these fluids would be released during the dehydration of serpentinites in the outermost part of the complex in contact with the granitic intrusion (e.g. Worden et al. 1991; Trommsdorff and Connolly 1996). Similar cases are seen where chromitite-bearing serpentinites have been thermally metamorphosed by the intrusion of plutonic rocks, producing core-to-rim zonation and different types of chromite zoning. These have been documented in some localities in Canada (Paktunç 1984), south-west Japan (Nozaka 2003 and references therein), Rio San Juan in the Dominican Republic (Saumur and Hattori 2013) and Calzadilla de los Barros in south-west Spain (Merinero et al. 2014).

The effects of metamorphic fluids on laurite stability

Experimental studies by Brenan and Andrews (2001), Andrews and Brenan (2002) and Bockrath et al. (2004a) showed that nearly pure laurite (RuS_2) with very low Os and Ir contents can form in equilibrium with Ru-poor Os–Ir alloys at chromian-spinel-based liquidus temperatures (1200 to 1300 °C) from S-undersaturated melts (log fS_2

from −2 to −1.3). These results also showed that if temperature raises above 1275 °C and/or fS_2 decreased, Ru–(Os–Ir) alloys can replace laurite (Brenan and Andrews 2001; Bockrath et al. 2004a), in consistency with the observation that PGE metal alloys can form as residual phases after sulphides are consumed by high degrees of partial melting (Peregoedova et al. 2004; Luguet et al. 2007; Fonseca et al. 2012). A similar transformation can occur if temperature drops down to 1180 °C at log $fS_2 = -2$, although the formation of Ru-bearing alloys can be achieved only when fS_2 is extremely low.

As noted above, the formation of Fe^{2+}-rich porous chromite in the chromitite at Loma Baya was concomitant with the serpentinization of olivine in the host rock (see also Fig. 6 in Gervilla et al. 2012). The hydration of olivine in the ultramafic rock produced antigorite and minor magnetite (Fig. 2b), thus releasing significant amounts of H_2 (e.g. Bach et al. 2006). In such an environment, magmatic sulphides tend to progressively equilibrate with H_2-rich fluids giving rise to S-deficient sulphides and PGE alloys (Eckstrand 1975; Frost 1985; Klein and Bach 2009; Debret et al. 2014; Foustoukos et al. 2015). As the edges of chromite developed porosity during the formation of Fe^{2+}-rich porous chromite, it is likely that H_2-rich fluids circulated through the interconnected network of pores and reacted with laurite grains that were originally hosted by primary chromite. This would cause reduction of laurite to Ru–(Os–Ir) alloy nanoparticles. Although the effect of pressure has not been constrained yet, the RuS_2/Ru° equilibrium curve obtained in low-pressure experiments (1GPa) show that under temperatures typical of Fe^{2+}-rich porous chromite formation (~330 °C), there is a congruent decomposition of RuS_2 to Ru° at ~log fS_2 of ~−18 (green star in Fig. 8). Foustoukos et al. (2015) obtained similar conditions of fS_2 (log $fS_2 = -20$) for the transformation $RuS_2 \Rightarrow$ Ru° in experiments conducted at 300 °C and 0.05 GPa, emphasizing that fO_2 does not significantly influence the speciation of PGEs, because PGE metals and alloys are stable under a great range to far more oxidizing conditions ($\gg fO_2$ haematite–magnetite buffer) than is usually found in hydrothermally altered peridotites.

Assuming that changes in pressure and fO_2 had no significant effect on RuS_2 stability at the given conditions for the alteration of the Loma Baya chromitites, it is likely that the occurrence of Ru–(Os–Ir) nanoparticles in cores and/or discrete bands (Fig. 4d, e) was the result of elemental rearrangement as laurite adjusted its composition via exsolution, in response to variations in T and fS_2 in the fluids responsible for alteration (e.g. Zaccarini et al. 2005; Kapsiotis et al. 2009). Even though some studies have provided experimental and empirical constrains for laurite crystallization from highly reducing fluids at infra-magmatic temperatures (Stockman and Hlava 1984; Wood 1987; Barkov and Fleet 2004; Garuti et al. 2007), the observation of laurite hosted in dark chromite cores (Fig. 4a) is consistent with a magmatic origin. Furthermore, our results do not support recrystallization of laurite at low temperature via the reaction of the already exsolved Ru–(Os–Ir) alloys with S when fS_2 increased in metasomatic fluids (e.g. González-Jiménez et al. 2010).

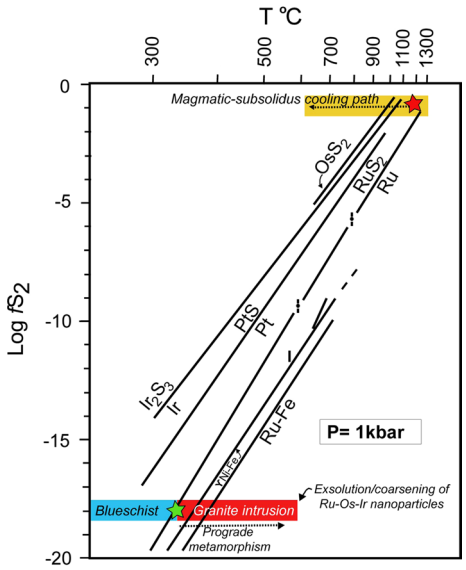

Fig. 8 Diagram of temperature versus sulphur fugacity (fS_2) for alloy-sulphide equilibrium (after Stockman and Hlava 1984). The *red star* indicates the conditions for the crystallization of laurite at the magmatic stage, whereas the *green star* indicates those for the reduction of laurite to Ru-alloy compound by infiltration of reducing fluids at the metamorphic peak in blueschist facies

Previous interpretations of the origin of primary Ru–(Os–Ir) alloys have been based exclusively on phase relations obtained from available experiments, which usually involve micrometre-sized phases (i.e. >1 μm in diameter). Below one micron, the number of available atoms becomes progressively limited as particle size decreases, which differs from classical thermodynamics, where the number of atoms is assumed to be unlimited (Wauteletl and Shirinyan 2009). For example, it is well known that a decrease in particle size to the nanoscale can promote phase instability due to the associated increase in surface energy; this ultimately implies that phase relations are also size- and shape dependent (McHale et al. 1997; Navrotsky 2001; Pohl et al. 2012). Further mineralogical changes in the mineral host at the micron to nanoscale during cooling, heating or fluid infiltration have a profound impact on the stability of noble-metal nanoparticles and hence will control their preservation in the geologic record. As recently documented for noble metals in iron sulphides (e.g. Deditius et al. 2009, 2011), the generation of nanoporosity and the formation of interconnected networks of nanofractures can alter mineral

structure and promote diffusional processes, thus enhancing segregation of noble-metal nanoparticles. This could be the case in the S-deficient laurites at Loma Baya, which exhibit cracks and porosity produced by volume changes associated with the reduction of the original sulphides to alloys at subsolidus conditions. Therefore, it is likely that mineralogical changes operating below the micron scale played a role in the formation and preservation of IPGE nanoparticles in laurites.

Genesis and preservation of Ru–(Os–Ir) nanoalloys in Loma Baya

At Loma Baya, laurite with different degrees of porosity contain nanoparticles of Ru–(Os–Ir) that exhibit various ranges of size distribution (e.g. normal versus bimodal distributions; Fig. 5a–c). This observation strongly suggests that solid-state, diffusion-driven particle coarsening or Ostwald-type ripening may have controlled nanoparticle stability during protracted metamorphism. Although Ostwald ripening has been previously proposed to operate at above the micron scale (e.g. garnet porphyroblasts; Miyazaki 1991, 1996), such coarsening processes are more efficient in the nanometre-scale realm, where diffusional fluxes are large enough to modify the distribution of nanoparticles (Carlson 1999; Reich et al. 2006; Becker et al. 2010).

In order to test this hypothesis, we have explored the thermal stability of Ru–(Os–Ir) nanoparticles hosted by a laurite-type mineral, by a critical assessment of the existing literature. No in situ heating transmission electron microscopy (TEM) data exist for this system, but the system Au–FeS_2 (Reich et al. 2006) may serve as an analogue to metal-nanoparticle stability in a refractory mineral medium. In broad terms, the bulk-melting temperature of Au (1064 °C) does not differ significantly from those of Ru–(Os–Ir) alloys (~1300 °C; Andrews and Brenan 2002; Fonseca et al. 2012). Also, despite differences in the thermodynamic stability and natural occurrence of laurite and pyrite, their structures are almost identical in terms unit cell parameters and symmetry (laurite, RuS_2, $a = 5.61$ Å, space group Pa3, Lutz et al. 1990; pyrite, FeS_2, $a = 5.42$ Å, space group Pa3, Bayliss 1977). Therefore, as first-order approximation, it might be reasonable to expect that the diffusion of noble metals would behave similarly in both structures. Coarsening and diffusional growth processes will be most likely controlled by (1) the energy due to dissolution of noble metals into the surrounding mineral host, (2) the loss of energy as the former nanoparticle–host interface is disrupted and (3) the cessation of intra-nanoparticle interactions (Reich et al. 2006; Becker et al. 2010).

Figure 8 shows a plot of temperature versus particle size constructed for noble-metal nanoparticles enclosed in a laurite-type mineral host. The thick red curve in this phase diagram represents the coarsening threshold for nanoparticles or diffusional boundary growth, which is broadly constrained here using recent datasets on noble-metal nanoparticles (Hills et al. 2003; Alyousef et al. 2010; So et al. 2010; Guisbiers et al. 2011; Cornish and Chown 2011). The lower limit (lower red curve) is defined by the temperature at which Os–Ir–Ru(–Pt) nanoalloys are stable during controlled heating (i.e. no significant growth at 300 °C for nanoparticles of ~4 nm; Alyousef et al. 2010). The upper limit of the growth boundary (upper red curve) for noble-metal nanoalloys is defined by the temperature–size relations at which coarsening is negligible within a reducing medium (~700 °C for sizes > ~10 nm; Alyousef et al. 2009; Prestat et al. 2013; Watanabe et al. 2013). Due to size-confinement quantum effects (Halperin 1986; Reich et al. 2011), both curves (and thus the whole diffusional growth boundary; red curved boundary area in Fig. 9) drop sharply at small particle sizes (left) and increase steadily towards the right until "bulk" conditions are reached at particle sizes of ~1 μm or larger (far right or point "7" in Fig. 9). In such a phase diagram, for any temperature and particle-size combination above the diffusional growth boundary (i.e. the "NPs unstable" field, in white) Ru–(Os–Ir) nanoparticles will not be stable unless coarsening occurs (horizontal black arrows); i.e. the growing particles will cross the diffusional growth boundary and enter the metal-nanoparticle stability field (light brown lower field, "NPs stable"). Therefore, any metal nanoparticle that forms below the upper boundary will be stable and preserved upon cooling without coarsening.

The effect of temperature on the average size of noble-metal nanoparticle in laurite grains from Loma Baya, which follows potential trajectories after their high-temperature formation (~1250 °C; Brenan and Andrews 2001; Andrews and Brenan 2002), is shown in Fig. 9. Under magmatic conditions, laurite will form a homogeneous solid solution [(Ru,Os,Ir)S_2] with a high Ru/(Ru + Os + Ir) ratio, and any available Os and Ir will be "dissolved" into the laurite matrix (no nanoparticles present, point 1 in Fig. 9), as observed in high-temperature experiments (e.g. Bockrath et al. 2004a). This is consistent with the homogeneous nature of the laurite enclosed in the darkest unaltered cores of chromite (Fig. 4a), which lack observable (<20 nm) nanoparticles. As primary laurite cools to 200 °C (point 2, i.e. minimum temperature estimated here for initiation of metamorphism) with no fluid infiltration, no changes are expected in either chromite or laurite, and the original magmatic structure of the sulphide is preserved.

During prograde HP/LT metamorphism in greenschist-to-blueschist facies (200–330 °C), fluids released may have produced partial hydration of the ultramafic rocks and their hosted chromitite, thus promoting the desulphurization of laurite under highly reducing conditions (trajectory 2 ⇒ 3 in Fig. 9). This will progressively affect the laurite matrix

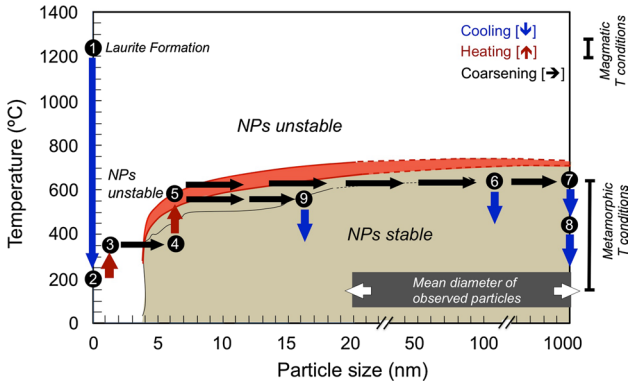

Fig. 9 Stability diagram for Ru–(Os–Ir) alloys as a function of temperature, particle size and mineral host (laurite-type structure). The thick red curve represents the nanoparticle coarsening threshold or diffusional growth boundary. Above this upper temperature limit (e.g. point 5), noble-metal nanoparticles in laurite are unstable unless coarsening occurs (black horizontal arrows). The *lower light brown field* represents the temperature versus size range of stability of nanoalloys (NPs stable). As a reference, the experimental curve for Au nanoparticle coarsening in refractory ore (Reich et al. 2006) is shown (*thin black curve*). See main text for details. Key: NP = nanoparticles

at the nanoscale and trigger the exsolution of Ru–(Os–Ir) nanoparticles due to, e.g., deviation from the ideal laurite stoichiometry as a result of desulphurization. Under this scenario, the first exsolved nanoalloys in the laurite matrix will be a few nanometre in size, as documented for nanoparticles exsolved from ABO_3 perovskites (e.g. Neagu et al. 2013). The exsolved nanoalloys will become unstable at such temperature–size conditions ("NP unstable" field in Fig. 9, e.g. point 3) unless they undergo coarsening by diffusion-driven, solid-state Ostwald ripening (black horizontal arrows) and cross the red boundary into the nanoparticle stability region ("NPs stable", Fig. 9). Assuming that exsolution and coarsening occur at this stage (path 3 ⇒ 4 in Fig. 9, at the conditions of the metamorphic peak at ~330 °C), nanoparticles will become stable after coarsening (point 4), and particle distributions with average sizes <10 nm will be preserved on cooling. However, this simplified trajectory does not satisfactorily explain the broad spread in Ru–(Os–Ir) nanometre-size distributions and textures observed at Loma Baya, i.e. variable particle sizes from tens of nm to 1 μm, and the different degrees of porosity and nanometre- to micrometre-scale veining (Fig. 5a–c).

A more reasonable scenario for metamorphic evolution at Loma Baya comprises an additional heating event associated with contact metamorphism after the hydrous metamorphism. As noted above, the peak of this thermal event is estimated to occur at 550–600 °C, at which the process of chromite alteration was inverted (point 5 in Fig. 9). Heating of the previously exsolved (and coarsened) nanoparticles of metal alloys during the prograde path (4 ⇒ 5 in Fig. 9) will dramatically affect nanoparticle stability (point 5). Thus, the exsolved Ru–(Os–Ir) alloy nanoparticles are not stable, and they will coarsen progressively until they reach average sizes of 100 nm (coarsening trajectory, from points 5–6). Considering that such prograde heating will affect the host rocks differentially (i.e. as a function of distance to heat source), it is likely that the wide spectrum of nanometre- to micrometre-sized particles observed in the laurites at Loma Baya reflects differential heating (horizontal range, lower right side of Fig. 9). This mechanism would allow significant coarsening of alloys in certain laurite grains (i.e. towards micron-scale path 7 ⇒ 8) while allowing the preservation of smaller nanoparticles in laurite grains that were less affected by heating (cooling from point 9).

Conclusions

The observed zoning in the Loma Baya chromites was produced during the polyphase metamorphism that affected the Loma Baya ultramafic complex. Porous rims of Fe^{2+}-rich chromite resulted from the hydrous alteration of magmatic chromite during greenschist-to-blueschist-facies metamorphism, whereas homogeneous chromite rims probably formed in response to a short-lived thermal event associated with an Eocene granite intrusion. Thermodynamic modelling in the CrMFASH system predicts the formation of Fe^{2+}-rich porous chromite in equilibrium with chlorite by hydration at 300 °C and 0.7 GPa, which coincides with the metamorphic peak as determined in metamorphic rocks spatially associated with the ultramafic rocks at Loma Baya. The Eocene thermal metamorphism induced by the granite intrusion reversed the alteration of chromite, thus producing new chromite with a composition close to the igneous one, in equilibrium with metamorphic (neoformed) olivine. The dehydration reaction is estimated to occur 550–600 °C, consistent with contact metamorphism produced by the intrusion of the Eocene granite. Our results show that chromite could record discrete metamorphic events (including recycling through a subduction zone to deep mantle regions or intrusions of hot plutonic bodies) in ultramafic rocks (preferentially containing chromitites) with complex, polymetamorphic histories. Such is the case especially if cooling rates are fast enough to prevent the complete obliteration of chemical and microstructural features in chromite caused by previous metamorphic events.

The changes that affected chromite during metamorphism had a profound impact on their hosted IPGE carriers. In particular, fluid infiltration under the reducing conditions in which Fe^{2+}-rich porous chromite formed promotes the reduction of the Ru-rich Os–Ir-bearing laurite to produce laurite progressively more S-deficient laurite while

exsolving nanoparticles of Ru–Os–Ir alloys. Using a temperature versus particle-size diagram constructed for noble-metal nanoparticles enclosed in a laurite-type mineral host, we show that these nm/μm Ru–(Os–Ir) particles did not form by cooling but by progressive heating during fluid-assisted prograde metamorphism. Further, the exsolution of such alloys is related to changes in the laurite structure (i.e. generation of nanopores) that promote diffusion, while the size, shape and preservation of the alloys are related to the thermal regime. At Loma Baya, the wide spectrum of nanometre- to micrometre-sized IPGE particles in laurite is the final result of differential heating.

The exsolution of nanometre- to micrometre-sized Ru–(Os–Ir) alloys in partly desulphurized laurite at Loma Baya was due to (and enhanced by) thermal metamorphism. This suggests that many of the nanoparticles documented in other partly desulphurized sulphides, which were interpreted as due to exsolution upon cooling, may instead be due to local thermal events related to contact or regional metamorphism. Therefore, interpretation of the origin of secondary Ru–Os–Ir alloys from many other geological suites may need to be reconsidered. In particular, the segregation of secondary Os-rich alloys may generate partly desulphurized sulphides with higher Re/Os ratios that over time will produce an excess of ^{187}Os, leading to potentially altered values for model ages and initial $^{187}Os/^{188}Os$ ratios in PGMs. As noted recently by Foustoukos et al. (2015), the recycling of these minerals back into the convecting mantle could result in locally high Pt/Os and Re/Os signatures that may explain heterogeneities in the osmium isotopic composition of the mantle.

Acknowledgments The authors acknowledge the critical review of Editor-in-Chief Othmar Müntener and two anonymous reviewers that greatly improved the final version of this manuscript. This research was supported by different funding sources, including a FONDECYT Initiation Grant #11140005 to J.M. González-Jiménez entitled "*Decoding precious metals (platinum-group elements and gold) in upper mantle rocks of the Chilean Cordillera*" and MSI "Millennium Nucleus for Metal Tracing along Subduction" (NC130065) headed by Martin Reich. Additional support was provided by a CONACYT grant to A. Camprubí (#155662) and a MEC grant to J. Proenza (CGL2012-36263). This is contribution 1022 from the ARC National Key Centre for Geochemical Evolution and Metallogeny of Continents (www.es.mq.edu.au/ GEMOC) and paper 650 from the ARC Centre of Excellence for Core to Crust Fluid Systems.

References

Ahmed AH, Hanghøj K, Kelemen PB, Hart SR, Arai S (2006) Osmium isotope systematics of the Proterozoic and Phanerozoic ophiolitic chromitites: in situ ion probe analysis of primary Os-rich PGM. Earth Planet Sci Lett 245:777–791

Alard O, Griffin WL, Lorand J-P, Jackson SE, O'Reilly SY (2000) Non-chondritic distribution of the highly siderophile elements in mantle sulphides. Nature 407:891–894

Alard O, Griffin WL, Pearson NJ, Lorand JP, O'Reilly SY (2002) New insights into the Re–Os systematics of sub-continental lithospheric mantle from in situ analysis of sulphides. Earth Planet Sci Lett 203:651–663

Alard O, Lorand JP, Reisberg L, Bodinier JL, Dutria JM, O'Reilly SY (2011) Volatile-rich metasomatism in Monteferrier xenoliths (Southern France): consequence for chalcophile and highly siderophile element abundance in an orogenic-type subcontinental mantle segment. J Petrol. doi:10.1093/petrology/egr038

Alyousef YM, Datta MK, Yao SC, Kumta PN (2009) Complexed sol–gel synthesis of improved Pt–Ru–Os-based anode electrocatalysts for direct methanol fuel cells. J Phys Chem Solids 70:1019–1023

Alyousef YM, Datta MK, Kadakia K, Yao SC, Kumta PN (2010) Sol–gel synthesis of Pt–Ru–Os–Ir based anode electro-catalysts for direct methanol fuel cells. J Alloys Compd 506:698–702

Andrews DRA, Brenan JM (2002) Phase-equilibrium constraints on the magmatic origin of laurite + Ru–Os–Ir alloy. Can Miner 40:1705–1716

Arai S (1975) Contact metamorphosed dunite-harzburgite complex in the Ghugoku district, western Japan. Contrib Miner Petrol 52:1–16

Arai S, Prichard HM, Matsumoto I, Fisher PC (1999) Potarite (Pd–Hg) in thermally metamorphosed dunite from the Inazumiyama ultramafic complex, southwestern Japan: an implication for the behaviour of mercury in PGE mineralization in peridotite. Miner Mag 63:369–377

Bach W, Paulick H, Garrido CJ, Ildefonse B, Meurer WP, Humphris SE (2006) Unraveling the sequence of serpentinization reactions: petrography, mineral chemistry, and petrophysics of serpentinites from MAR 15°Nn(ODP Leg 209, Site 1274). Geophys Res Lett 33:L13306

Ballhaus C, Bockrath C, Wohlgemuth-Ueberwasser C, Laurenz V, Berndt J (2006) Fractionation of the noble metals by physical processes. Contrib Miner Petrol 152:667–684

Barkov AY, Fleet ME (2004) An unusual association of hydrothermal platinum-group minerals from the Imandra layered complex, Kola Peninsula, northwestern Russia. Can Miner 42:455–467

Barnes SJ (2000) Chromite in komatiites, II. Modification during greenschist to mid-amphibolite facies metamorphism. J Petrol 41(3):387

Barnes SJ, Fiorentini ML (2008) Iridium, ruthenium and rhodium in komatiites: evidence for iridium alloy saturation. Chem Geol 257:44–58

Barnes SJ, Roeder PL (2001) The range of spinel compositions in terrestrial mafic and ultramafic rocks. J Petrol 42(12):2279

Barra F, Gervilla F, Hernández E, Reich M, Padrón-Navarta JA (2014) Altered chromian spinels from La Cabaña peridotite, south central Chile: considerations on the formation of ferritchromite. Miner Petrol. doi:10.1007/S00710-014-0335-5

Bayliss P (1977) Crystal structure refinement of a weakly anisotropic pyrite cubic model. Am Miner 62:1168–1172

Becker U, Reich M, Biswas S (2010) Nanoparticle-host interactions in natural systems. In: Brenker FE, Jordan G (eds) Nanoscopic approaches in earth and planetary sciences, Chap 8, vol 8. EMU notes in mineralogy. European Mineralogical Union and The Mineralogical Society of Great Britain and Ireland, Cambridge, pp 325–376

Bliss NW, MacLean WH (1975) The paragenesis of zoned chromite from central Manitoba. Geochim Cosmochim Acta 39:973–990

Bockrath C, Ballhaus C, Holzheid A (2004a) Stabilities of laurite RuS_2 and monosulphide liquid solution at magmatic temperature. Chem Geol 208:265–271

Bockrath C, Ballhaus C, Holzheid A (2004b) Fractionation of the platinum-group elements during mantle melting. Science 305:1951–1953

Brenan JM (2002) Re–Os Fractionation in Magmatic Sulfide Melt by Monosulfide Solid Solution. Earth Planet Sci Lett 199:257–268

Brenan JM, Andrews D (2001) High-temperature stability of Laurite and Ru–Os–Ir alloy and their role in PGE fractionation in mafic magmas. Can Miner 39:341–360

Burkhard DJM (1993) Accessory chromium spinels: their coexistence and alteration in serpentinites. Geochim Cosmochim Acta 57:1297–1306

Camprubí A (2013) Tectonic and metallogenic history of Mexico. In: Colpron M, Bissig T, Rusk BG, Thompson JFH (eds) Tectonics, metallogeny, and discovery: the North American Cordillera and similar accretionary settings. Special publication 17. Society of Economic Geologists, Denver, pp 201–243

Carlson WD (1999) The case against Otswald ripening of porphyroblasts. Can Miner 37:403–413

Connolly JAD (2009) The geodynamic equation of state: what and how. Geochem Geophys Geosyst 10:Q10014. doi:10.1029/2009GC002540

Centeno-García E, Busby C, Busby M, Gehrels G (2011) Evolution of the Guerrero composite terrane along the Mexican margin, from extensional fringing arc to contractional continental arc. Geol Soc Am Bull 123:1776–1797

Cornish LA, Chown LH (2011) Platinum-based alloys and coatings: materials for the future? Adv Gas Turbine Technology, Dr. Ernesto Benini (ed), ISBN: 978-953-307-611-9, InTech, doi:10.5772/19886

Debret B, Andreani M, Muñoz M, Bofan-Casanova N, Carlut J, Nicollet C, Schwartz S, Trcera N (2014) Evolution of Fe redox state in serpentinite during subduction. Earth Planet Sci Lett 400:206–218

Deditius A, Utsunomiya Reich M, Kesler SE, Ewing RC, Hough R, Walshe EJ (2011) Trace metal nanoparticles in pyrite. Ore Geol Rev 42:32–46

Delgado-Argote LA, López-Martínez M, York D, Hall CM (1992) Geologic framework and geochronology of ultramafic complexes of southern Mexico. Can J Earth Sci 29:1590–1604

Dick HJB, Bullen T (1984) Chromian spinel as petrogenetic indicator in abyssal and alpine-type peridotites and spatially associated lavas. Contrib Miner Petrol 86:54–76

Eckstrand OR (1975) The Dumont Serpentinite: a model for control of nickeliferous opaque mineral assemblages by alteration reactions in ultramafic rocks. Econ Geol 70:183–201

Engi M (1983) Equilibra involving Al–Cr spinel: Mg–Fe Exchange with olivine. Experiments, thermodynamic analysis, and consequences of geothermometry. Am J Sci 283A:20–71

Evans BW, Frost BR (1975) Chrome-spinel in progressive metamorphism—a preliminary analysis. Geochim Cosmochim Acta 39:959–972

Evans BW, Johannes W, Oterdoom H, Trommsdorff V (1976) Stability of chrysotile and antigorite in the serpentinite multisystem. Schweiz Miner Petrogr Mitt 56:79–93

Ferrari L, Bergomi M, Martini M, Tunesi A, Orozco-Esquivel T, López-Martínez M (2014) Late Cretaceous-Oligocene magmatic record in southern Mexico: the case for a temporal slab window along the evolving Caribbean-North America-Farallon triple boundary. Tectonics 33:1738–1765

Finnigan CS, Brenan JM, Mungall JE, McDonough WF (2008) Experiments and models bearing on the role of chromite as a collector of platinum group minerals by local reduction. J Petrol 49:1647–1665

Fonseca ROC, Laurenz V, Mallmann G, Luguet A, Hoehne N, Jochum KP (2012) New constrains on the genesis and long-term stability of Os-rich alloys in the Earth's mantle. Geochim Cosmochim Acta 87:227–242

Foustoukos DI, Bizimis M, Frisby C, Shirey SB (2015) Redox controls on Ni-Fe-PGE mineralization and Re/Os fractionation during serpentinization of abyssal peridotite. Geochim Cosmochim Acta 150:11–25

Frost BR (1975) Contact metamorphism on serpentinite, chloritic blackwall and rodingite at Paddy-Go-Easy Pass, Central Cascades, Washington. J Petrol 16(2):272–313

Frost BR (1985) On the stability of sulfides, oxides and native metals in serpentinite. J Petrol 25:31–63

Frost BR, Beard J (2007) On silica activity and serpentinization. J Petrol 48:1351–1368

Frost BR, Evans KA, Swapp SM, Beard JS, Mothersole FE (2013) The process of serpentinization in dunite from New Caledonia. Lithos 178:24–39

Garuti G, Zaccarini F (1997) In situ alteration of platinum-group minerals at low temperature : evidence from serpentinized and weathered chromitite of the Vourinos complex, Greece. Can Miner 35:611–626

Garuti G, Proenza JA, Zaccarini F (2007) Distribution and mineralogy of platinum-group elements in altered chromitites of the Campo Formoso layered intrusión (Bahia State, Brazil): control by magmatic and hydrothermal processes. Miner Petrol 89:159–188

Gervilla F, Padrón-Navarta JA, Kerestedjian T, Sergeeva I, González-Jiménez JM, Fanlo I (2012) Formation of ferrian chromite in podiform chromitites from the Golyamo Kamenyane serpentinite, Eastern Rhodopes, SE Bulgaria: a two-stage process. Contrib Miner Petrol 164:643–657

Ghorfi ML, Melcher F, Oberthür T, Boukhari AE, Maacha L, Maddi A, Mhaili M (2008) Platinum group minerals in podiform chromitites of the Bou Azzer ophiolite, Anti Atlas, Central Morocco. Miner Petrol 92:59–80

Golding HG, Bayliss P (1968) Altered cromite ores from the Coolac serpentine belt Neew South Wales, Australia. Am Miner 53:162–183

González-Jiménez JM, Kerestedjian T, Proenza JA, Gervilla F (2009) Metamorphism on chromite ores from the Dobromirtsi ultramafic massif, Rhodope mountains (SE Bulgaria). Geol Acta 7:413–429

González-Jiménez JM, Gervilla F, Kerestedjian T, Proenza JA (2010) Effects of meta-morphism on platinum-group and base-metal mineral assemblages in ophiolite chromitites from the Dobromirtsi massif, Rhodope Mountains (SE Bulgaria). Res Geol 60(4):315–334

González-Jiménez JM, Gervilla F, Griffin WL, Proenza JA, Augé T, O'Reilly SY, Pearson NJ (2012a) Os-isotope variability within sulfides from podiform chromitites. Chem Geol 291:224–235

González-Jiménez JM, Griffin WL, Gervilla F, Kerestedjian TN, O'Reilly SY, Proenza JA, Pearson NJ, Sergeeva I (2012b) Metamorphism disturbs the Re–Os signatures of platinum-group minerals in ophiolite chromitites. Geology. http://dx.doi.org/10.1130/G33064.1

González-Jiménez JM, Marchesi C, Griffin WL, Gutiérrez-Narbona R, Lorand J-P, O'Reilly SY, Garrido CJ, Gervilla F, Pearson NJ, Hidas K (2013a) Transfer of Os isotopic signatures from peridotite to chromitite in the subcontinental mantle: insights from in situ analysis of platinum-group and base-metal minerals (Ojén peridotite massif, southern Spain). Lithos 164-167:74–85

González-Jiménez JM, Locmelis M, Belousova E, Griffin WL, Gervilla F, Kerestedjian T, O'Reilly SY, Sergeeva I, Pearson NJ (2013b) Genesis and tectonic implications of podiform chromitites in the metamorphosed Ultramafic Massif of Dobromirtsi (Bulgaria). Gondwana Res 27:555–574. doi:10.1016/j.gr.2013.09.020

González-Jiménez JM, Griffin WL, Gervilla F, Proenza JA, O'Reilly SY, Pearson NJ (2014) Chromitites in ophiolites: how, where, when, why? Part I. Origin and significance of platinum-group minerals. Lithos 189:127–139

Guisbiers G, Abudukelimu G, Hourlier D (2011) Size-dependent catalytic and melting properties of platinum-palladium nanoparticles. Nanoscale Res Lett 6:396

Halperin WP (1986) Quantum size effects in metal particles. Rev Mod Physics 58:533–606

Helmy HM, Ballhaus C, Fonseca ROC, Wirth R, Nagel T, Tredoux M (2013) Noble metal nanoclusters and nanoparticles precede mineral formation in magmatic sulfide melts. Nat Commun 4:2405. doi:10.1038/ncomms3405

Hills CW, Mack NH, Nuzzo RG (2003) The size-dependent structural phase behaviors of supported bimetallic (Pt–Ru) nanoparticles. J Phys Chem B 107:2626–2636

Hochella MF Jr, Lower SK, Maurice PA, Penn RL, Sahai N, Sparks DL, Twining BS (2008) Nanominerals, mineral nanoparticles, and earth systems. Science 319:1631–1635

Holland TJB, Powell R (1998) An internally consistent thermodynamic data set for phases of petrological interest. J Metamor Geol 16:309–343

Hutchinson D, Prichard HM, Macleod CJ (1999) Evidence for partial melting and melt impregnation of mantle peridotites leading to PGM deposition: a comparison of samples from the Lizard and Troodos ophiolites and the Tonga Trench [abs.]. In: Stanley CJ et al (eds) Mineral deposits: Processes to processing: Rotterdam. Balkema, SGA London, pp 729–732

Jöns N, Bach W, Klein F (2010) Magmatic influence on reaction paths and element transport during serpentinization. Chem Geol 274:196–211

Junge M, Wirth R, Oberthür T, Melcher F, Schreiber A (2015) Mineralogical sitting of platinum-group elements in pentlandite from the Bushveld Complex, South Africa. Miner Depos 50:41–54

Kapsiotis A, Grammatikopoulos TA, Tsikouras B, Hatzipanagiotou K (2009) Chromian spinel composition and platinum-group element mineralogy of chromitites from the Milia Area, Pindos ophiolite complex, Greece. Can Miner 47:1037–1056

Khedr MZ, Arai S (2010) Hydrous peridotites with Ti-rich chromian spinel as a low-temperature forearc mantle facies: evidence from the Happo-O'ne meta- peridotites (Japan). Contrib Miner Petrol 159:137–157

Khedr MZ, Arai S (2012) Petrology and geochemistry of prograde deserpentinized peridotites from Happo-O'ne, Japan: evidence of element mobility during deserpentinization. J Asian Earth Sci 43:150–163

Klein F, Bach W (2009) Fe–Ni–Co–O–S phase relations in peridotite-seawater interactions. J Petrol 50:37–59

Klemme S, Ivanic TJ, Connolly JAD, Harte B (2009) Thermodynamic modelling of Cr-bearing garnets with implications for diamond inclusions and peridotite xenoliths. Lithos 112:986–991

Kogiso T, Suzuki K, Suzuki T, Uesugi K (2008) Two- and three-dimensional imaging of platinum-group minerals at submicrometer scale with synchrotron X-ray. Goldschmidt conference abstracts, p 1212

Leblanc M, Nicolas A (1992) Ophiolitic chromitites. Int Geol Rev 34:653–686

Lorand JP, Pattou L, Gros M (1999) Fractionation of platinum group element in the upper mantle: a detailed study in Pyrenean orogenic lherzolites. J Petrol 40:957–981

Lorand JP, Alard O, Luguet A (2010) Platinum-group element micronuggets and refertilization process in Lherz orogenic peridotite (northeastern Pyrenees, France). Earth Planet Sci Lett 289:298–310

Luguet A, Alard O, Lorand J-P, Pearson NJ, Ryan CG, O'Reilly SY (2001) LAM-ICPMS unravel the highly siderophile element geochemistry of abyssal peridotites. Earth Planet Sci Lett 189:285–294

Luguet A, Lorand JP, Alard O, Cottin JY (2004) A multi-technique study of platinum-group elements systematic in some Ligurian ophiolitic peridotites, Italy. Chem Geol 208:175–194

Luguet A, Shirey S, Lorand JP, Horan MF, Carlson RC (2007) Residual platinum- group minerals from highly depleted harzburgites of the Lherz massif (France) and their role in HSE fractionation of the mantle. Geochim Cosmochim Acta 71:3082–3097

Lutz HD, Muller B, Schmidt T, Stingl T (1990) Structure refinement of pyrite-type ruthenium disulfide, RuS_2, and ruthenium diselenide, $RuSe_2$. Acta Crystallogr A C46:2003–2005

Malitch KN (2004) Osmium isotope constraints on contrasting sources and prolonged melting in the Proterozoic upper mantle: evidence from ophiolitic Ru–Os sulfides and Ru–Os–Ir alloys. Chem Geol 208:157–173

Marchesi C, González-Jiménez JM, Gervilla F, Garrido CJ, Griffin WL, O'Reilly SY, Proenza JA, Pearson NJ (2011) In situ Re–Os isotopic analysis of platinum-group minerals from the Mayarí-Cristal ophiolitic massif (Mayarí–Baracoa Ophiolitic Belt, eastern Cuba): implications for the origin of Os-isotope heterogeneities in podiform chromitites. Contrib Miner Petrol 161:977–990

Matthes S, Knauer E (1981) The phase petrology of the contact metamorphic serpentinite near Erbendorf, Oberpfalz, Bavaia. Neues Jahrb Geol Palaontol Abh 141:59–89

McElduff B, Stumpfl EF (1990) Platinum-group minerals from the troodos ophiolite, Cyprus. Mineral Perol 42:211–232

McHale JM, Auroux A, Perrotta AJ, Navrotsky A (1997) Surface energies and thermodynamic phase stability in nanocrystalline aluminas. Science 277:788–791

Mellini M, Rumori C, Viti C (2005) Hydrothermally reset magmatic spinels in retrograde serpentinites: formation of "ferritchromit" rims and chlorite aureoles. Contrib Miner Petrol 149(3):266–275

Mendoza OT (2000) Pre-accretion metamorphism of the Teloloapan Terrane (southern Mexico): example of burial metamorphism in an island-arc setting. J South Am Earth Sci 13:337–354

Mendoza OT, Suastegui MG (2000) Geochemistry and isotopic composition of the Guerrero Terrane (western Mexico): implication for the tectono-magmatic evolution of southwestern North America during the Late Mesozoic. J South Am Earth Sci 13:297–324

Merinero R, Lunar R, Ortega L, Piña R, Monterrubio S, Gervilla F (2014) Zoned chromite records multiple metamorphic episodes in the Calzadilla de los Barros ultramafic bodies (SW Iberian Peninsula). Eur J Miner. doi:10.1127/ejm/2014/0026-2406

Merlini A, Grieco G, Diella V (2009) Ferritchromite and chromian-chlorite formation in mélange-hosted Kalkan chromitite (Southern Urals, Russia). Am Miner 94(10):1459–1467

Mitchell RH, Keays RR (1981) Abundance and distribution of gold, palladium and iridium in some spinel garnet lherzolites: implications for the nature and origin of precious metal, sulfur-rich intergrannular components in the upper mantle. Geochim Cosmochim Acta 45:425–2442

Miyazaki K (1991) Ostwald ripening of garnet in high *P/T* metamorphic rocks. Contrib Mineral Petrol 108:118–128

Miyazaki K (1996) A numerical simulation of textural evolution due to Ostwald ripening in metamorphic rocks: a case for small amount of volume of dispersed crystals. Geochim Cosmochim Acta 60:277–290

Mondal SK, Frei R, Ripley E (2007) Os isotope systematics of mesoarchean chromitite-PGE deposits in the Singhbhum Craton (India): implications for the evolution of the lithospheric mantle. Chem Geol 244:391–408

Mukherjee R, Mondal SK, Rosing MT, Frei R (2010) Compositional variations in the Mesoarchean chromites of the Nuggihalli schist belt, Western Dharwar Craton (India): potential parental melts and implications for tectonic setting. Contrib Miner Petrol 160(6):865–885

Mungall JE (2002) Kinetic controls on the partitioning of trace elements between silicate and sulfide liquids. J Petrol 43:749–768

Nagaya T, Wallis SR, Kobayashi H, Michibayashi K, Mizukami T, Seto Y, Miyake A, Matsumoto M (2014) Dehydration breakdown of antigorite and the formation of B-type olivine CPO. Earth Planet Sci Lett 387:67–76

Nakagawa M, Franco HEA (1997) Placer Os–Ir–Ru alloys and sulphides: indicators of sulphur fugacity in an ophiolite? Can Miner 35:1441–1452

Navrotsky A (2001) Thermochemistry of nanomaterials. Rev Mineral Geochem 44:73–103

Neagu D, Tsekouras G, Miller DN, Ménard H, Irvine JTS (2013) In situ growth of nanoparticles through control of non-stoichiometry. Nat Chem 5(916):923

Nilsson LP (1990) Platinum-group mineral inclusions in chromitite from the Osthammeren ultramafic tectonite body, south central Norway. Miner Petrol 42:249–263

Nozaka T (2003) Compositional heterogeneity of olivine in thermally metamorphosed serpentinite from Southwest Japan. Am Miner 88:1377–1384

Ohnenstetter M (1992) Platinum-group element enrichment in the upper mantle peridotites of the Monte Maggiore ophiolitic massif (Corsica, France): Mineralogical evidence for ore-forming metasomatism. Miner Petrol 46:85–107

Oka Y, Steinke P, Chatterjee N (1984) Thermodynamic mixing properties of $Mg(Al, Cr)_2O_4t$; spinel crystalline solution at high temperatures and pressures. Contrib Miner Petrol 87:196–204

Ortiz-Hernández LE, Escamilla-Casas JC, Flores-Castro K, Ramírez-Cardona M, Acevedo-Sandoval O (2006) Características geológicas y potencial metalogenético de los principales complejos ultramáficos-máficos de México. Boletín de la Sociedad Geológica Mexicana 57:161–181

Padrón-Navarta JA, Hermann J, Garrido CJ, López Sánchez-Vizcaíno V, Gómez-Pugnaire MT (2010) An experimental investigation of antigorite dehydration in natural silica-enriched serpentinite. Contrib Mineral Petrol 159:25–42

Paktunç A (1984) Metamorphism of the ultramafic rocks of the Thompson Mine, Thompson Nickel Betlt, Northern Manitoba. Can Mineral 22:77–91

Park JW, Campbell IH, Arculus RJ (2013) Platinum-alloy and sulfur saturation in an arc-related basalt to rhyolite suite: evidence from the Pual Ridge lavas, the Eastern Manus Basin. Geochim Cosmochim Acta 101:76–95

Peregoedova A, Barnes SJ, Baker DR (2004) The formation of Pt–Ir alloys and Cu–Pd-rich sulfide melts by partial desulfurization of Fe–Ni–Cu sulfides: results of experiments and implications for natural systems. Chem Geol 208:247–264

Pohl J, Stahl C, Albe K (2012) Size-dependent phase diagrams of metallic alloys: a Monte Carlo simulation study on order-disorder transitions in Pt–Rh nanoparticles. Eilstein Journal of Nanotechnology 3:1–11

Prestat E, Ropescu R, Blank H, Schneider R, Gerthsen D (2013) Coarsening of Pt nanoparticles on amorphous carbon film. Surf Sci 609:195–202

Prichard HM, Tarkian M (1988) Platinum and palladium minerals from two PGE-rich localities in the Shetland ophiolite complex. Can Miner 26:979–990

Prichard HM, Ixer RA, Lord RA, Maynard J, Williams N (1994) Assemblages of platinum-group minerals and sulfides in silicate lithologies and chromite-rich rocks within the Shetland ophiolite. Can Miner 32:271–294

Prichard HM, Neary CR, Fisher FC, O'Hara MJ (2008) PGE-rich Podiform chromitites in the Al'Ays ophiolite complex, Saudi Arabia: an example of critical mantle melting to extract and concentrate PGE. Econ Geol 103:1507–1529

Proenza J, Ortega-Gutiérrez F, Camprubí A, Tritlla J, Elías-Herrera M, Reyes-Salas M (2004) Paleozoic serpentinite-enclosed chromitites from Tehuitzingo (Acatlán Complex, southern Mexico): a petrological and mineralogical study. J South Am Earh Sci 16(8):649–666

Proenza JA, Zaccarini F, Lewis JF, Longo F, Garuti G (2007) Chromian spinel composition and the platinum-group minerals of the PGE-rich Loma Peguera chromitites, Loma Caribe peridotite, Dominican Republic. Can Miner 45:631–648

Pruseth KL, Palme H (2004) The solubility of Pt in liquid Fe-sulfides. Chem Geol 208:233–245

Rëhkamper M, Halliday AN, Fitton JG, Lee DC, Wieneke M, Arndt NT (1999) Ir, Ru, Pt, and Pd in basalts and komatiites: new constraints for the geochemical behaviour of the platinum-group elements in the mantle. Geochim Cosmochim Acta 63:3915–3934

Reich M, Utsunomiya S, Kesler S, Wang L, Ewing RC, Becker U (2006) Thermal behaviour of metal nanoparticles in geologic materials. Geology 34(12):1033–1036

Reich M, Hough R, Deitius A, Utsunomiya S, Ciobanu C, Cook NJ (2011) Nanogeoscience in ore system research: principles, methods and applications. Ore Geol Rev 42:1–5

Salgado-Terán V, Serrano-Villar JF (1983) Estudio geológico del yacimiento de níquel y cromo en rocas ultrabásicas, municipios de Petatlán y Tecpan, estado de Guerrero. Unpublished BSc dissertation, Facultad de Ingeniería, Universidad Nacional Autónoma de México, Distrito Federal, Mexico, 65 p

Saumur BM, Hattori K (2013) Zoned Cr-spinel and ferritchromite alteration in forearc mantle serpentinites of the Rio San Juan Complex, Dominican Republic. Miner Mag 77(117):136

SCENIHR (2010) Scientific Basis for the Definition of the Term "nanomaterial", ISSN 1831-4783 ISBN 978-92-79-12757-1, doi:10.2772/39703 ND-AS-09-004-EN-N

Schneider CA, Rasband WS, Eliceiri KW (2012) NIH Image to ImageJ: 25 years of image analysis. Nat Methods 9:671–675

Shi R, Alard O, Zhi X, O'Reilly SY, Pearson NJ, Griffin WL, Zhang M, Chen X (2007) Multiple events in the Neo-Tethyan oceanic upper mantle: evidence from Ru–Os–Ir alloys in the Luobusa and Dongqiao ophiolitic podiform chromitites. Tibet. Earth Planet Sci Lett 261:33–48

So MH, Ho CH, Chen R, Che CM (2010) Hydrothermal synthesis of platinum-group-metal nanoparticles by using HEPES as a reductant and stabilizer. Chem Asian J 5:1322–1331

Springer RK (1974) Contact metamorphosed ultramafic rocks in the western Sierra Nevada foothills, California. J Petrol 15:160–195

Stockman HW, Hlava PF (1984) Platinum-group minerals in Alpine chromitites from southwestern Oregon. Econ Geol 79:492–508

Suita MT, Streider AJ (1996) Cr-spinels from Brazilian mafic–ultramafic complexes: metamorphic modifications. Int Geol Rev 38:245–267

Thalhammer OAR, Prochaska W, Mühlhans HW (1990) Solid inclusions in chrome- spinels and platinum group element concentration from the Hochgrössen and Kraubath Ultramafic Massifs (Austria). Contrib Miner Petrol 105:66–80

Torres-Ruiz J, Garuti G, Gazzotti M, Gervilla F, Fenoll Hach-Alí P (1996) Platinum- group minerals in chromitites from the Ojen lherzolite massif (Serranía de Ronda, Betic Cordillera, Southern Spain). Miner Petrol 56:25–50

Tredoux M, Lindsay NM, Davies G, McDonald L (1995) The fractionation of platinum-group elements in magmatic systems, with the suggestion of a novel causal mechanism. S Afr J Geol 98:157–167

Trommsdorff V, Connolly AD (1996) The ultramafic contact aureole about the Bregaglia (Bergell) tonalite: isograds and a thermal model. Schweiz Miner Petrorg Mitt 76:537–547

Trommsdorff V, Evans BW (1972) Progressive metamorphism of antigorite schist in the Bergell tonalite aureole (Italy). Am J Sci 272:423–437

Trommsdorff V, Evans BW (1974) Alpine metamorphism of peridotitic rocks. Schweiz Miner Petrogr Mitt 54:333–352

Ulmer P, Trommsdorff V (1995) Serpentine stability to mantle depths and subduction-related magmatism. Science 268:858–861

Ulmer P, Trommsdorff V (1999) Phase relations of hydrous mantle subducting to 300 km. Mantle petrology: field observations and high pressure experimentation: a tribute to Francis R, (Joe) Boyd. The Geochemical Society, Spetial Publication, p 6

Wang KL, O'Reilly SY, Griffin WL, Pearson NJ, Zhang M (2009) Sulfides in mantle peridotites from Penghu Island, Taiwan: melt percolation, PGE fractionation, and the lithospheric evolution of the South China block. Geochim Cosmochim Acta 73:4531–4557

Watanabe M, Akimoto T, Kondoh E (2013) Synthesis of platinum-ruthenium alloy nanoparticles on carbon using supercritical fluid deposition. ECS J Solid State Sci Technol 2(1):M9–M12

Wauteletl M, Shirinyan AS (2009) Thermodynamics: nano vs. Macro. Pure Appl Chem 81(10):1921–1930

Wirth R, Reid D, Schreiber A (2013) Nanometer-sized platinum-group minerals (PGM) in base metal sulfides: new evidence for an orthomagmatic origin of the Merensky Reef PGE ore deposit, Bushveld Complex, South Africa. Can Miner 51:143–155

Wood S (1987) Thermodyamic calculations of the volatility of the platinum group elements (PGE): the PGE content of fluids at magmatic temperatures. Geochim Cosmochim Acta 51:3041–3050

Worden RH, Droop GTR, Champness PE (1991) The reaction antigorite → olivine + talc + H_2O in the Bergell aureole N. Italy. Miner Mag 55:367–377

Wylie AG, Candela PA, Burke TM (1987) Compositional zoning in unusual Zn-rich chromite from the Sykesville district of Maryland and its bearing on the origin of ¨ferritchromit¨. Am Miner 72:413–422

Zaccarini F, Proenza JA, Ortega-Gutiérrez F, Garuti G (2005) Platinum group minerals in ophiolitic chromitites from Tehuitzingo (Acatlán complex, southern Mexico): implications for post-magmatic modification. Miner Petrol 84:147–168